Controls on Bending-Related Faulting Offshore of the Alaska Peninsula

Jacob Clarke[1,2]; Donna J. Shillington[1], Christine Regalla[1]; James B. Gaherty[1]; Justin Estep[1], Douglas A. Wiens[3], Anne Bécel[4], Mladen R. Nedimović[5]

[1]Northern Arizona University, School of Earth and Sustainability, Flagstaff, AZ USA
[2]Southern Methodist University, Dallas, TX, USA
[3]Washington University in St Louis, St Louis, MO USA
[4]Lamont-Doherty Earth Observatory of Columbia University, Palisades, NY USA
[5]Dalhousie University, Halifax, NS, Canada

Corresponding author: Jacob Clarke

Key Points:

- Bathymetry data reveal variations in the orientation and summed throws of bending faulting outboard of the Alaska subduction zone
- Westward increase in number and summed throws of bending faults is due to favorably oriented pre-existing structures and increased slab dip
- Variable orientations of bend faulting and volcanic constructs updip of 2020 M7.6 intraplate earthquake implies complex stresses in the slab

Abstract

Oceanic plates experience extensive normal faulting as they bend and subduct, enabling fracturing of the incoming lithosphere. Debate remains about the relative importance of pre-existing faults, plate curvature and other factors controlling the extent and style of bending-related faulting. The subduction zone off the Alaska Peninsula is an ideal place to investigate controls on bending faulting as the orientation of abyssal-hill fabric with respect to the trench and plate curvature vary along the margin. Here we characterize faulting between longitudes 161°W and 155ºW using newly collected multibeam bathymetry data. We also use a compilation of seismic reflection data to constrain patterns of sediment thickness on the incoming plate. Although sediment thickness increases over 1 km from 156°W to 160°W, most sediments were deposited prior to the onset of bending faulting and thus should have limited impact on the expression of bend-related fault strikes and throws in bathymetry data. Where magnetic anomalies trend subparallel to the trench (<30°) west of ~156ºW, bending faults parallel magnetic anomalies, implying bending faults reactivate pre-existing structures. Where magnetic anomalies are highly oblique (>30°) to the trench east of 156ºW, no bending faults are observed. Summed fault throws increase to the west, including where pre-existing structure orientations are constant (between 157-161ºW), suggesting that another factor such as the increase in slab curvature must influence bending faulting. However, the westward increase in summed fault throws is more abrupt than expected for gradual changes in slab bending, alone, suggesting potential feedbacks between pre-existing structures, slab dip, and faulting.

Plain Language Summary

Subduction zones are plate boundaries where two tectonic plates converge, and the oceanic plate is bent and forced to below the other plate. Oceanic plates are faulted as they bend, and these "bending faults" are thought to be important for controlling the deep water cycle on Earth and influencing the generation of large earthquakes in subduction zones. The amount and style of bending faulting varies between and within subduction zones around the world, and debate remains about what causes this variability. Possible controls include the overall curvature of the oceanic plate as it bends and subducts and pre-existing weaknesses in the oceanic plate from when it formed. We use bathymetry data across the Alaska subduction zone to characterize bending faults here and understand controls on their formation. This is an ideal study area because the curvature of the plate and the pre-existing weaknesses vary in this region. The amount of bending faulting increases abruptly to the west and appears to result from a feedback between favorably oriented pre-existing weaknesses and increased curvature of the oceanic plate. These results can be used to understanding bending faulting in other subduction zones.

1 Introduction

Bending and loading of the subducting oceanic lithosphere at subduction zones causes the crust and upper mantle to flex, forming a bulge seaward of the trench that has been termed the outer rise (Bodine & Watts, 1979; Caldwell et al., 1976; Garcia et al., 2019). Flexure of the incoming plate and negative buoyancy of the downwelling slab puts the upper portion of the lithosphere under extension and results in normal faulting in the incoming plate (Chapple & Forsyth, 1979; Faccenda, 2014; Ranero et al., 2003). These normal faults, known as bending-related faults, are found at subduction zones around the globe and occur between the trench axis and outer-rise (Hilde, 1983; Masson, 1991). Bending-related faults form between the trench and outer-rise, and slip occurs on these faults both prior to subduction as the plate approaches the plate interface and post-subduction as the plate bends, and eventually unbends and dehydrates (e.g., Ranero et al., 2005).

Faulting of downgoing slabs prior to subduction is thought to have several influences on subduction processes: 1) faults provide pathways for seawater infiltration into and hydration of the oceanic lithosphere (Cai et al., 2018; Contreras-Reyes et al., 2008; Faccenda, 2014; Fujie et al., 2018; Hacker, 2008; Van Keken et al., 2011; Wei et al., 2021); 2) bending-related faulting contributes to frictional heterogeneity on the megathrust once subducted (Wang & Bilek, 2014); and 3) faults host normal-faulting earthquakes both outboard and within the subduction zone (Lay et al., 2009, 2011; Ranero et al., 2005). Water has been interpreted to be stored in the upper mantle of the downgoing plate (e.g., Cai et al., 2018; Grevemeyer et al., 2018; Ivandic et al., 2008; Lefeldt et al., 2012; Ranero et al., 2003; Shillington et al., 2015) in the form of serpentinite, the hydrous alteration of peridotite in the upper mantle. Water can also be stored as pore fluids in fault zones in the crust and mantle of the incoming plate, and contained in seafloor sediments (Canales et al., 2017; Faccenda, 2014; Iyer et al., 2012; Miller et al., 2021). The breakdown of serpentinite and release of water at depth could influence pore fluid pressures along the megathrust interface (Hasegawa & Nakajima, 2017; Peacock, 2001), the volume and composition of arc magmatism (e.g., Wei et al., 2021), and the occurrence of intermediate depth earthquakes (Boneh et al., 2019; Kita et al., 2006; Ranero et al., 2005; Shillington et al., 2015; Wei et al., 2021). Therefore, better knowledge on the controls on bending-related faulting formation, fault throws, and lateral extent can lead to further understanding of the subduction water cycle, earthquakes, and magmatism.

Although the existence of these faults at subduction zones is well documented, the style and magnitude of faulting vary between and within subduction zones (e.g., Contreras-Reyes et al., 2008; Eimer et al., 2020; Fujie et al., 2018; Kobayashi et al., 1995, 1998; Obana et al., 2019; Ogawa et al., 1997; Ranero et al., 2003; Van Avendonk et al., 2011). Thus, questions remain on the primary controls on bending faulting. Possible controls include plate curvature (Naliboff et al., 2013; Nishikawa & Ide, 2015) and/or pre-existing structures (Fujie et al., 2018; Ranero et al., 2003; Shillington et al., 2015). The curvature of the slab is correlated with the elastic thickness of the plate, which is largely determined by the slab age (Bodine & Watts, 1979; Pérez-Gussinyé et al., 2008). Additionally, fracturing due to bending of the downwelling slab and resulting serpentinization of the upper mantle may weaken the slab, allowing for more bending and hence further faulting (Contreras-Reyes & Osses, 2010).

In this study, we use a compilation of multibeam bathymetry data, including recently acquired data from the Alaska Amphibious Community Seismic Experiment (AACSE) in 2018-2019 (Barcheck et al., 2020), to characterize bending-related faults in detail, including orientations, lengths, spacing, and scarp heights. To test models for controls on faulting, we compare these bending-fault characteristics with the orientations of pre-existing abyssal-hill faults from magnetic data, orientation of the trench, and changes in dip of the incoming plate along strike.

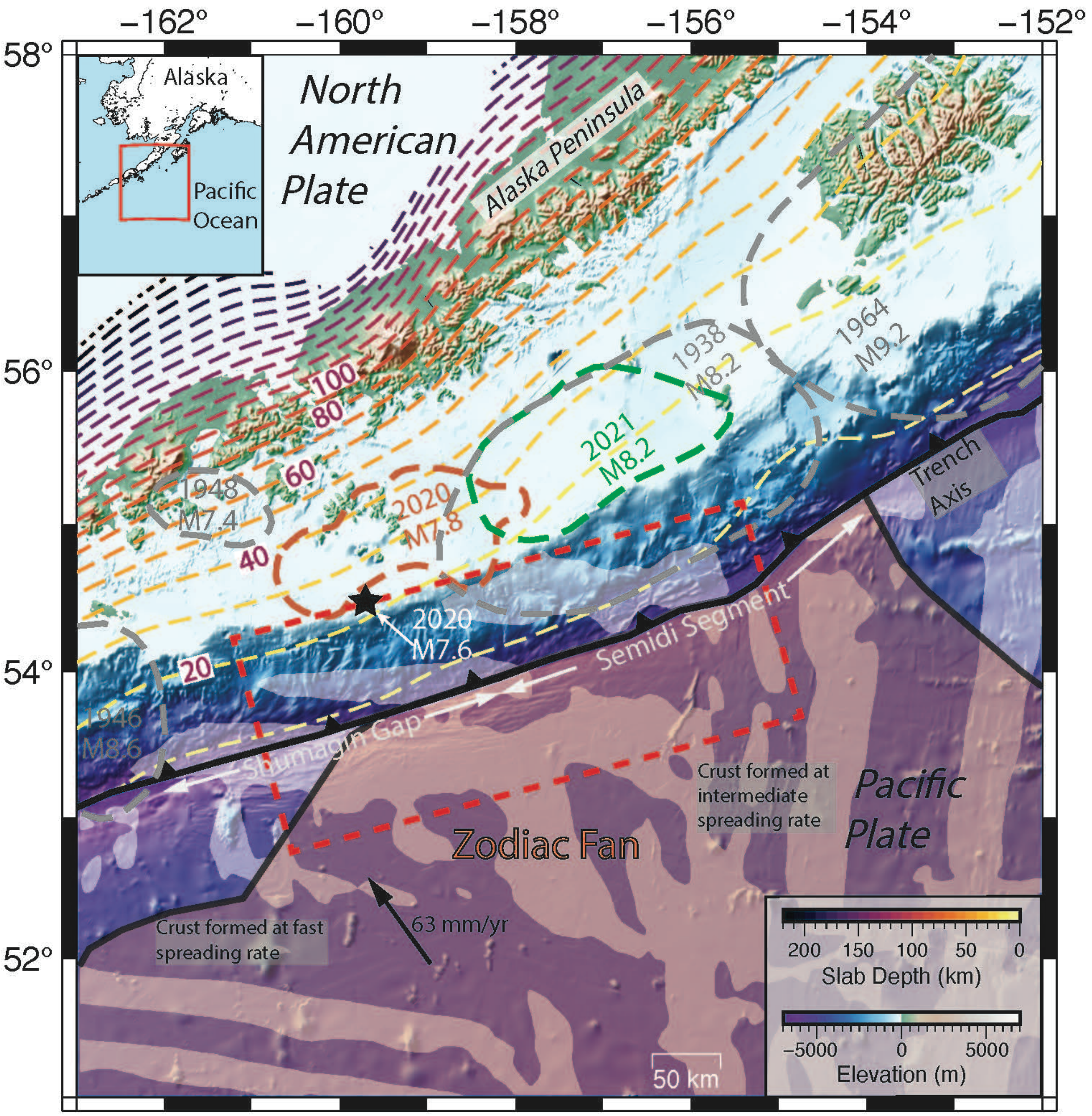

Figure 1: Map of study area with historic large rupture zones (gray dotted outlines, Davies et al., 1981), 2020 M7.8 rupture (orange dotted outline, Xiao et al., 2021), 2021 M8.2 Chignik rupture (green dotted outline, Elliot et al., 2022), 2020 M7.6 intraplate event centroid (black star), trench axis (solid barbed black line, Bassett & Watts, 2015), magnetic anomalies (positive anomalies shown with white patches on incoming Pacific plate, Maus et al., 2009) slab depth contours (colored dotted lines – 10 km contours, Hayes et al., 2018), and sediments derived from the Zodiac Fan (orange shaded area, von Huene et al., 2012). Primary study area with new high-resolution bathymetry data (dashed red box) between longitudes 155-161°W. Convergence rate from Sella et al., (2002) shown with black arrow and text. Inset shows study area location.

2 Tectonic Background

The subduction zone offshore of the Alaska Peninsula is an ideal location to examine controls on the formation of bending-related faulting (Fig. 1). The subducting plate has an age of ~55 Ma throughout the study area (Lonsdale et al., 1988) and is subducting nearly orthogonally at a rate of 63 mm/yr (Sella et al., 2002). The strike of the trench axis also remains relatively uniform at an azimuth of ~70° through the study area, which spans longitudes 155-161°W. The consistent plate age, trench axis strike, and convergence rate leads to a nearly constant thermal structure of the subduction zone.

Although the age and convergence direction are constant, the dip of the slab and orientation of pre-existing structures vary along strike. The dip of the slab steepens from the Gulf of Alaska west to the Aleutians, including steepening between the eastern Semidi segment, longitudes ~155-159°W, and the western Shumagin Gap, longitudes ~159-162°W (Hayes et al., 2018; Kuehn, 2019; Fig. 1). One possible cause for the eastward shallowing of the slab is the subduction of an oceanic plateau (the Yakutat block) in the easternmost part of Alaska subduction zone; the buoyancy resulting from the thickened crust is thought to contribute to shallow slab subduction there (Worthington et al., 2012). Another possible cause for westward increase in the slab dip is a transition from oceanic/continental subduction to oceanic/oceanic subduction; west of the primary study region, the subduction zone transitions to an oceanic/oceanic margin which may promote stab steepening (Holt et al., 2015; Sharples et al., 2014).

The spreading history of the incoming oceanic crust also varies along strike, separated by a remnant triple junction marking the relict Kula, Pacific, Farallon triple junction (Engebretson et al., 1985; Lonsdale, 1988). The remnant triple junction appears as a T-shaped feature in the magnetic data at ~158°W (Fig. 1). Cessation of spreading at this triple junction occurred between ~43-44 Ma (Engebretson et al., 1985; Lonsdale, 1988). Oceanic crust formed from Kula-Pacific spreading is currently subducting in the Shumagin Gap (~159-162°W) and western Semidi segment (~155-159°W). This crust formed at fast spreading rates (half rates of ~74 mm/yr, Engebretson et al., 1985), and magnetic anomalies trend slightly oblique to the trench axis by ~20°. Oceanic crust in the eastern Semidi segment formed from Pacific-Farallon spreading at intermediate rates (half rates of ~28-34 mm/yr, Engebretson et al., 1985). Magnetic anomalies in this crust trend ~N-S and highly oblique to the trench (~70°). Tectonic reconstructions by Fuston & Wu (2020) suggest the possible existence of a Resurrection plate and Kula-Resurrection ridge striking N-S that would have subducted beneath the Alaska Peninsula. The proposed Kula-Resurrection ridge would have been active from ~60-40 Ma.

Previous work, based on lower-resolution bathymetry data along the Alaska-Aleutian trench that largely focused on a region further west than our primary study area, identified a connection between the trends of magnetic anomalies and strikes of bending-related faults (Masson, 1991; Mortera-Gutiérrez et al., 2003). Masson (1991) showed the angle between pre-existing abyssal-hills inferred from magnetic anomalies plays a key role in whether bending reactivates abyssal-hills or forms new faults, including in the Alaska-Aleutian subduction. In the western Aleutians, between 179°E and 169°W, analysis of bathymetry data shows that fault strikes closely follow the oceanic spreading fabric which is near parallel to the trench (<10° difference) (Masson, 1991;

Mortera-Gutiérrez et al., 2003). Between 157ºW and 169°W, bending faults show two strikes: one primary set following the inherited spreading fabric, and a secondary set parallel to the trench axis (Masson, 1991). The angle between the trench and abyssal-hill faults is up to 30° in that region, and bending fault orientations suggest both reactivation of inherited weaknesses and the formation of new bending faults paralleling the trench.

Shillington et al. (2015) used 2D active-source seismic transects to show that the incoming plate outboard of the Shumagin Gap (~159-162°W) is more pervasively faulted than outboard of the Semidi segment (~155-159°W). They also found that the upper mantle of the slab has a larger area of reduced seismic velocities seaward of the Shumagin Gap compared to the Semidi segment, which they attributed to an increase in hydration and associated serpentinization to the west. The incoming plate outboard of the Shumagin Gap also has greater total seismicity, which could suggest a greater number of bending-related faults (Shillington et al., 2015).

In addition to possible along-strike changes in bending faulting and resulting hydration, the Alaska peninsula also exhibits changes in coupling (Drooff & Freymueller, 2021; Li & Freymueller, 2018), great earthquake history (Davies et al., 1981), seismicity at a range of depths (Shillington et al., 2015; Wei et al., 2021), and arc chemistry (Buurman et al., 2014; Wei et al., 2021), all of which have been proposed to be influenced by faulting and hydration of the incoming plate. The Semidi segment has a history of generating great (M > 8.0) earthquakes with a recurrence interval of ~50-75 years (Davies et al., 1981), including the recent M8.2 Chignik earthquake in July 2021 in the western part of the Semidi segment (e.g., Elliott et al., 2022; Liu et al., 2022). GPS measurements show that the Semidi segment is highly locked overall and that locking increases to the east (Drooff & Freymueller, 2021; Li & Freymueller, 2018; Zhao et al., 2022). The Shumagin Gap, however, is only weakly coupled (<30% coupled). Great earthquakes along the megathrust appear to be less common in the Shumagin Gap, with the last occurring in 1847 or possibly 1788 (Davies et al., 1981). However, the eastern part of the deep Shumagin Gap did recently rupture in a M7.8 earthquake in July 2020 (Liu et al., 2022; Xiao et al., 2021) and hosted an intraplate M7.6 earthquake in October 2020 (Zhou et al., 2022). Greater roughness at the top of the subducting plate due to increased bending faulting (e.g., Li et al., 2018; Wang & Bilek, 2014) and fluids from the hydrated lithosphere (Cordell et al., 2023; Li & Freymueller, 2018) have been proposed to contribute to changes in locking and earthquake history.

There are also along-strike changes in intermediate depth earthquakes (Shillington et al., 2015) and calculated *b*-values (Wei et al., 2021). Florez & Prieto (2019) showed that subduction zones with high *b*-values (a comparitively greater ratio of small earthquakes to large earthquakes) suggest greater extent of dehydration reaction, and thus more water stored in the downgoing plate. The Semidi segment is characterized by a double-seismic zone with moderate *b*-values and few earthquakes extending deeper than 100 km (Abers, 1992; Wei et al., 2021). This suggests that that the volume of water stored in the downgoing slab through bending faults at this segment is less than other subduction segments to the west. High *b*-value earthquakes in the Shumagin Gap extend to depths >200 km, implying greater amounts of water stored here (Wei et al., 2021). Finally, trace element geochemistry at volcanic centers in the Shumagin and Semidi segments show that sediment input of source magmas is higher at the Semidi segment and water input is less (Wei et al., 2021).

3 Data and Methods

We map and characterize bending faults on the incoming plate offshore of the Alaska Peninsula using a compilation of existing bathymetry data. Recently deposited sediments have the potential to mask the bathymetric expression of bending faults so, where it is available, we use existing seismic reflection data to map the total sediment thickness and thickness of sediment deposited near the trench axis during bending faulting, which we call trench fill. Finally, to examine possible controls on bending-related faulting, we use the trends of magnetic anomalies to estimate the strike of pre-existing faults and fractures, and used profiles of depth to top of igneous crust and bathymetry to calculate the dip of the incoming plate outboard of the trench.

3.1 Characterizing bending faulting in bathymetry data

We map bending-related faults between longitudes 161-155°W (Fig. 2) using new high-resolution multibeam bathymetry data collected as part of AACSE (Barcheck et al., 2020) combined with other existing bathymetric data (Ryan et al., 2009; Fig. 2). The combined data provide nearly complete, continuous coverage of an area spanning roughly 100x300 km with a 125-m grid resolution, forming an excellent basis for systematic identification and characterization (geometry and displacement) of faults based on their surface expression. While bathymetry data are limited due to their inability to quantify faults in the subsurface, the seismic datasets that enable subsurface quantification of faults (Section 3.3) are too incomplete to allow for a comprehensive characterization of the entire region.

The mapped region encompasses the incoming plate subducting in the Shumagin Gap (159-162°W) and Semidi segment (155-159°W). Previous efforts to examine bending faults offshore of the Alaska Peninsula used lower resolution (~200 m) GLORIA and Seabeam swath data (Scanlon & Masson, 1992) or spatially limited swath data from modern sonar systems (Shillington et al., 2015). The availability of new high-resolution bathymetry area provides the opportunity to map faults in greater detail and extent. Faults are mapped by hand using a processed bathymetry grid that is detrended and demeaned to produce relative elevation, which removes long-wavelength variations and highlights faulting (Fig. 2, Supplementary Fig S-8). Detrending is done by applying a cosine bandpass filter with corners at 10000/3000/1000/100 m. These values have been chosen based on the average and minimum spacings between bending-related faults. Only faults with minimum scarps of ±5 m in the detrended grid are included in this mapping effort.

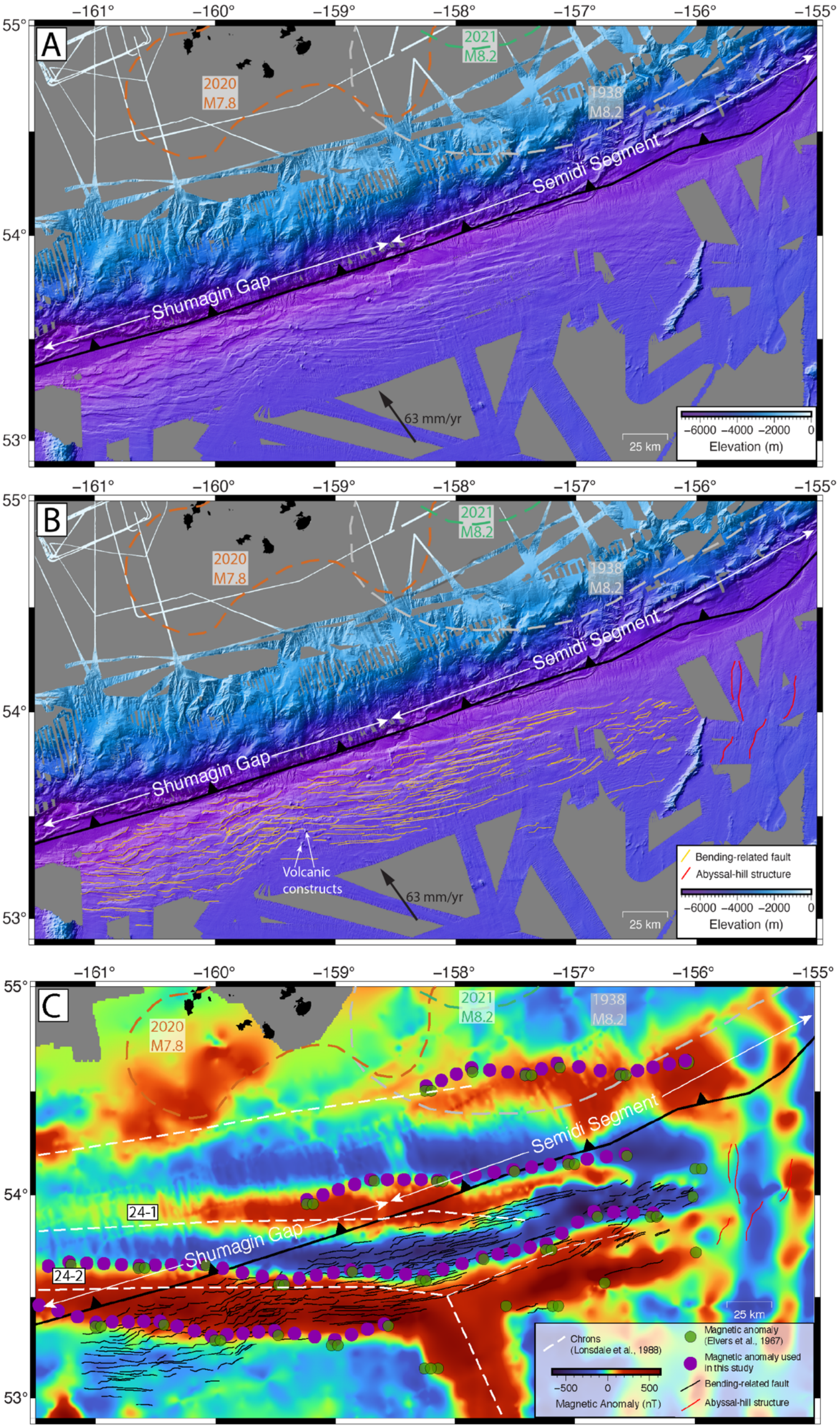
A
B
C
−161°
−160°
−159°
−158°
−157°
−156°
−155°
55°
54°
53°
2020
M7.8
2021
M8.2
1938
M8.2
Semidi Segment
Shumagin Gap
63 mm/yr
25 km
−6000 −4000 −2000 0
Elevation (m)
Volcanic constructs
Bending-related fault
Abyssal-hill structure
24-1
24-2
Chrons
(Lonsdale et al., 1988)
−500 0 500
Magnetic Anomaly (nT)
Magnetic anomaly
(Elvers et al., 1967)
Magnetic anomaly used in this study
Bending-related fault
Abyssal-hill structure

Figure 2: A) New high-resolution bathymetry data (Barcheck et al., 2020; Ryan et al., 2009). Gray areas show regions without swath bathymetry coverage. The trench axis (Bassett & Watts, 2015) is shown by the thick black line in all panels. B) Interpreted bathymetry data with mapped bending-related faults (yellow). Red lines in the eastern part of the study area that are oriented N-S are interpreted to show remnant abyssal-hill structures and not active bending-related faults. Rupture patches are shown on the overriding plate with colors matching those shown in Fig. 1. C) Mapped bending-related faults (thin black lines) overlain on magnetic anomaly grid (Bankey et al., 2002). Note the rotation in spreading direction from N-S west of ~156ºW to E-W east of ~156ºW. White dashed lines and boxed annotations show magnetic chrons based on interpretations from Lonsdale et al. (1988). A remnant triple junction can be observed at 158ºW. Green dots show magnetic anomaly picks from Elvers et al. (1967) used as a guide for magnetic anomaly picks presented in this study (larger purple points). Notice the apparent absence of bending faults at the seafloor east of ~156°W (and not at the triple junction), where orientations of magnetic anomalies change. Magnetic anomaly orientations do not change at the triple junction due to a plate reorganization that occurred ~53 Ma (Lonsdale, 1988).

Each mapped fault trace is resampled to 100-m intervals along-strike. We measure fault strike, fault dip direction (seaward or trenchward), and distance from the trench for each 100 m segment. We examine variations in bending fault strike along the subduction zone by calculated histograms of fault azimuth in 1º longitude wide bins (i.e., 156-157ºW, 157-158ºW, etc., Fig. 3).

The maximum throw for each fault is estimated using a 4-km-long bathymetric profile orthogonal to the fault. The position of this profile was selected at the location along the fault estimated to have the maximum scarp height. Linear regression of hand-picked points from the bathymetric profile is used to calculate slope and 95% confidence intervals for the hanging wall and footwall seafloor surfaces. These surfaces are then used to calculate the vertical separation by subtracting elevations of the hanging wall surface from the footwall surface at a range of positions that could represent the intersection of the fault plane with the scarp face. The throw is calucated from vertical separation by assuming a dip of 60º (Figs. S-1, S-2). We use this approach because it accounts for variations in the bathymetric slope of the footwall and hanging wall, which is particularly important within 30 km of the trench where bending is the most severe. To examine along-strike variations in the total amount of fault slip, maximum throw estimates are summed within 0.5º-wide bins. We utilized 0.5º-wide bins to achieve relatively high resolution in the along strike variations in summed fault throws, while still having enough faults in each bin. We note that varying the bin size does not impact the observed trends.

3.2 Estimating strikes of pre-existing structures from magnetic anomaly data

Inherited abyssal-hill fabric within oceanic plates can be estimated from magnetic anomalies, where abyssal-hill faults are expected to form parallel to the mid-ocean ridge due to normal faulting (e.g., Macdonald et al., 1996), and thus parallel to the trend of magnetic anomalies. Elvers et al. (1967) map isochrons in detail on the subducting Pacific plate in our study area. To estimate the likely orientation of pre-existing faults in our study area, we resample picks made by Elvers et al. (1967) (which closely follows magnetic anomaly peaks of the North American magnetic anomaly map created by Bankey et al. (2002)) to 1 km. Based on these magnetic anomaly picks, we estimate the strikes and standard deviations of abyssal-hill faults that may be reactivated during slab bending in 1º wide bins using four distinct anomalies in the study area (Figs. 2C, 3). We compare these data to the trend of the trench axis of Bassett & Watts (2015).

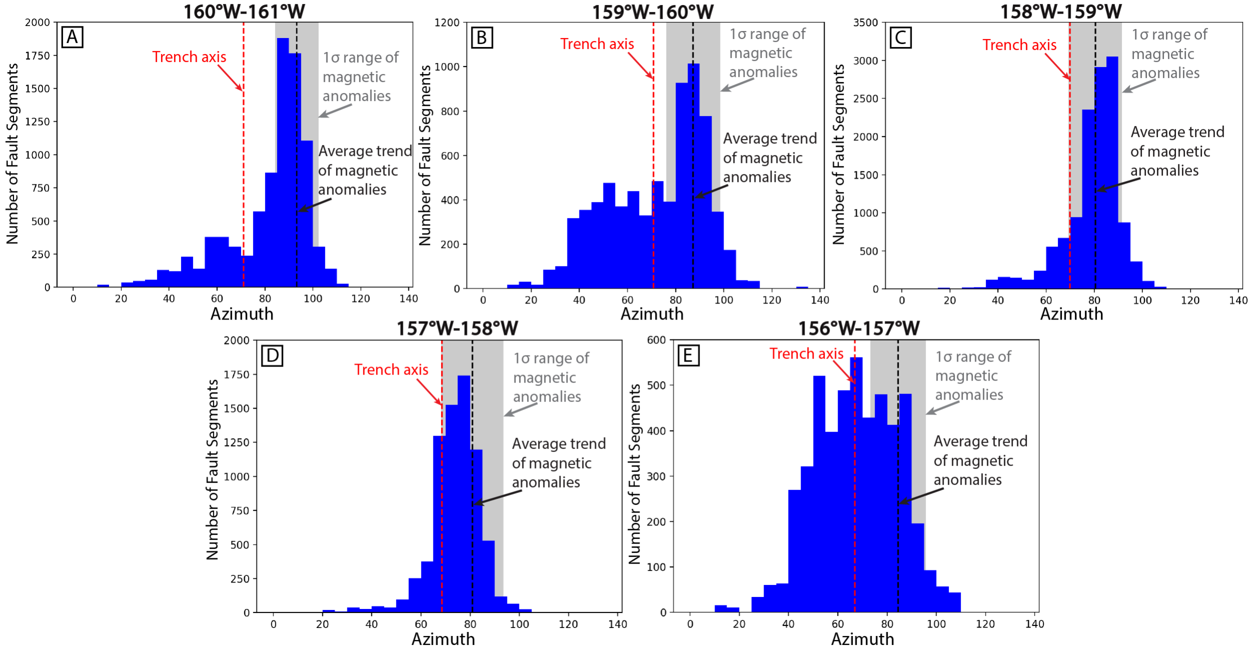

Figure 3: Histograms comparing fault segment strike azimuths (blue bars) in 1-degree bins with the average trend of the trench (red dotted line, Bassett & Watts, 2015) and average trend of magnetic anomalies (black dotted line). One-standard-deviation range of magnetic anomalies is shown by the gray box in the background. Dominant peaks of fault strikes primarily follow the trend of magnetic anomalies (panels A, C, D). Between 159-160ºW (panel B), fault strike azimuths show one dominant trend following magnetic anomalies, and a secondary trend ranging from ~35-80º. Between 156-157ºW, there are fewer faults with a broader distribution of strike azimuths (panel E). Note that vertical axis varies between panels.

3.3 Sediment thickness and basement offsets from seismic reflection data

We compile seismic reflection data collected on the incoming plate from the National Archive of Marine Seismic Surveys (NAMSS, Triezenberg et al., 2016), the ALEUT experiment (Bécel et al., 2015, 2017; Kuehn, 2019; Li et al., 2015) and the AACSE experiment (Barcheck et al., 2020; Bécel et al., 2019) to determine total sediment thickness and the thickness of sediments within the trench throughout the study area (Fig. 4). Previous studies have documented along-strike changes in sediment thickness on the incoming plate, with larger sediment thickness offshore of the Semidi segment (Straume et al., 2019). The thickness of trench fill sediments also varies along the margin (e.g., von Huene et al., 2012), and this portion of the sedimentary section has the highest potential to mask bending faults because it was deposited during the time of bending fault formation and development. We pick arrival times for the seafloor, base of trench fill, and top of igneous crust on time migrated profiles (Fig. 5). The top of igneous crust is marked by an irregular bright reflector arising from the contrast between sediments and the basalts of Layer 2A. Sediments deposited on the incoming plate outboard of the trench consists of pelagic sediments and terrigenous fan sediments of the Zodiac fan (Creager et al, 1973; Stevenson et al., 1983; von Huene et al., 2012). These sediment layers generally parallel the underlying oceanic crust on the incoming plate and reflectors within these deposits can be traced out of the trench onto the incoming plate. These can be distinguished from trench fill sediments, which are restricted to the trench axis, flat laying, and uncomformably overlay incoming sediments. Trench fill sediments are deposited primarily by along-axis flow of sediment from the northeast (von Huene et al., 2012).

Subtracting the seafloor from the base of trench fill and from the top of igneous crust provides thickness in two-way travel time of the trench fill and total sediment section, respectively. We convert time to depth using a velocity of 1.8 km/s; this average velocity is based on seismic processing of ALEUT reflection data (Bécel et al., 2015). We use a single velocity for depth conversion due to uncertainty in both spatial distribution and depth-dependent velocities for each of the three sediment packages on the incoming plate: pelagic sediments, terrigenous fan sediments, and Quaternary trench fill (Creager et al., 1973; Stevenson et al., 1983; von Huene et al., 2012). These uncertainties obviate the benefit of using a depth-dependent velocity for conversion. To create a grid of total sediment thickness and trench fill on the incoming Pacific plate, we grid the resulting sediment thickness values using a nearest neighbor algorithm with a 100-km radius and 0.1° grid spacing (Fig 4).

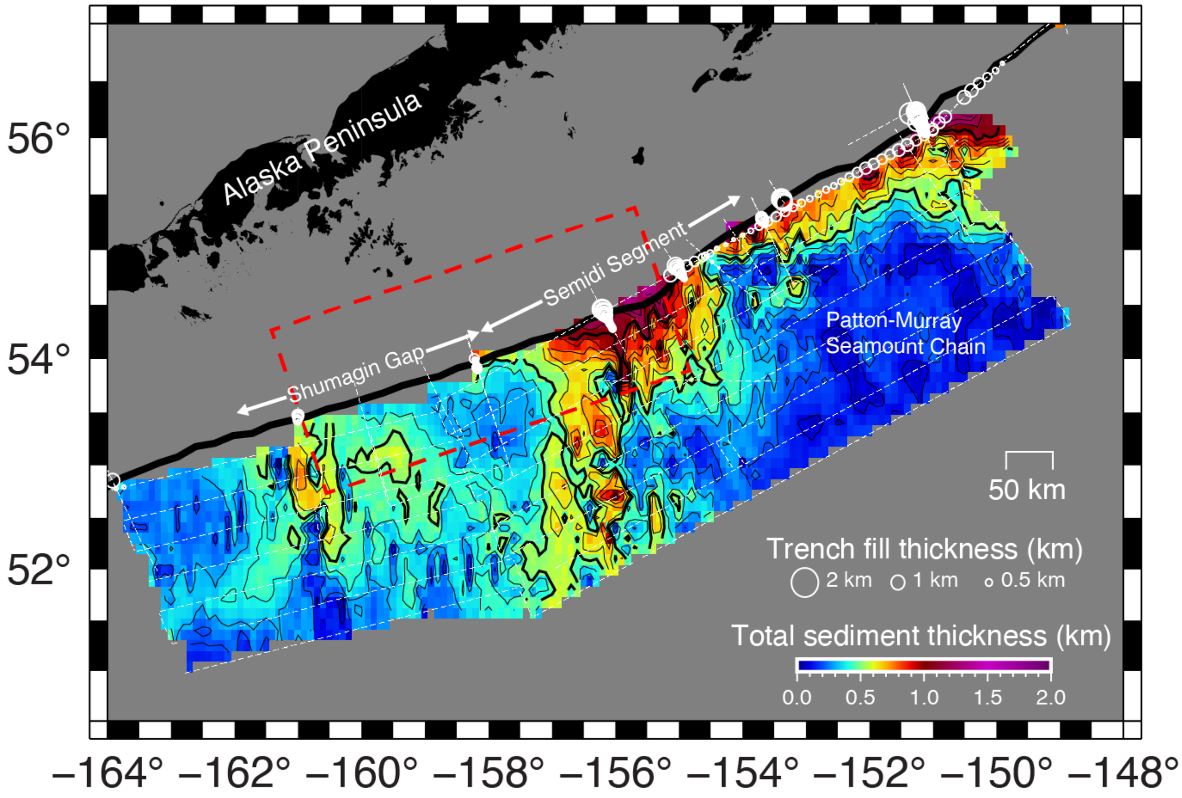

Figure 4: Map of gridded sediment thickness based on legacy single-channel USGS seismic reflection lines (Triezenberg et al., 2016) and multi-channel seismic reflection lines from ALEUT (Bécel et al., 2015, 2017; Kuehn, 2019; Li et al., 2015) and AACSE (Bécel et al. 2019). Seismic profiles are indicated by dashed white lines. The thickness of trench fill is indicated with open circles sized by thickness. The absence of a trench fill circle for trench-perpendicular lines represents a thickness of zero. Primary study area shown by dashed red box as in Fig. 1.

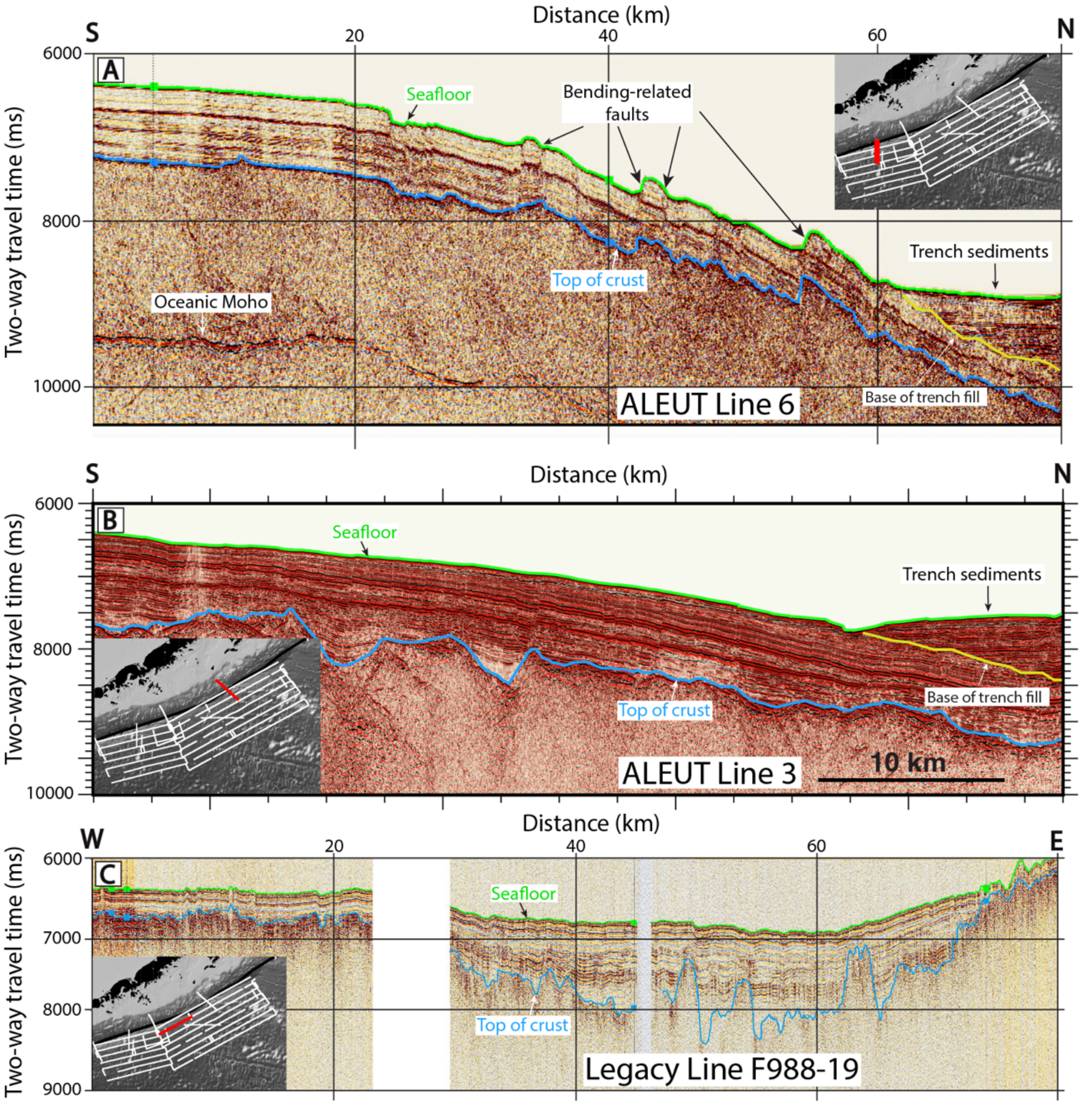

Figure 5: Examples of seismic reflection profiles A) outboard of the Shumagin Gap (ALEUT line 6) showing extensive bending faulting at the seafloor and top of the crust (Bécel et al., 2017) and B) Outboard of the Semidi Segment, with few to no bending fault expressions in the sediments or at the top of the crust (Shillington et al., 2015). Insets show seismic line locations highlighted in red. Topography in the top of crust outboard of the Semidi segment (panel B) is largely caused by the formation of crust at moderate spreading rates, which creates a more faulted crust surface at formation than fast spreading rates offshore of the Shumagin Gap, and these features are likely not active bending-faulting. There is little evidence of faulting-caused deformation in the sediments in this region and observable deformation may be caused by differential compaction. C) Roughly trench-parallel seismic reflection profile F988-19 (Triezenberg et al., 2016) showing the westward decrease in sediment thickness. Note the rougher crust surface to the east, also mentioned in panel B, created by slower spreading rates.

3.4 Estimating bending angle from bathymetry data and seismic reflection profiles

The dip of the slab at depth increases along strike (e.g., Hayes et al., 2018; Kuehn, 2019), and we seek to evaluate the contribution of changes in slab bending to observed patterns of faulting. We create a grid of the depth to top of igneous crust by subtracting the grid of sediment thickness described in section 3.3 from the bathymetry grid. We calculate the dip of the incoming plate near the trench by applying linear regression of 50-km-long trench-perpendicular profiles of the top of igneous crust (Fig. 6) following the method of Nishikawa & Ide (2015). For comparison, we also estimate dip of the seafloor along the same profiles using the same bathymetry data as the fault mapping analysis (Figs. 7, S-6).

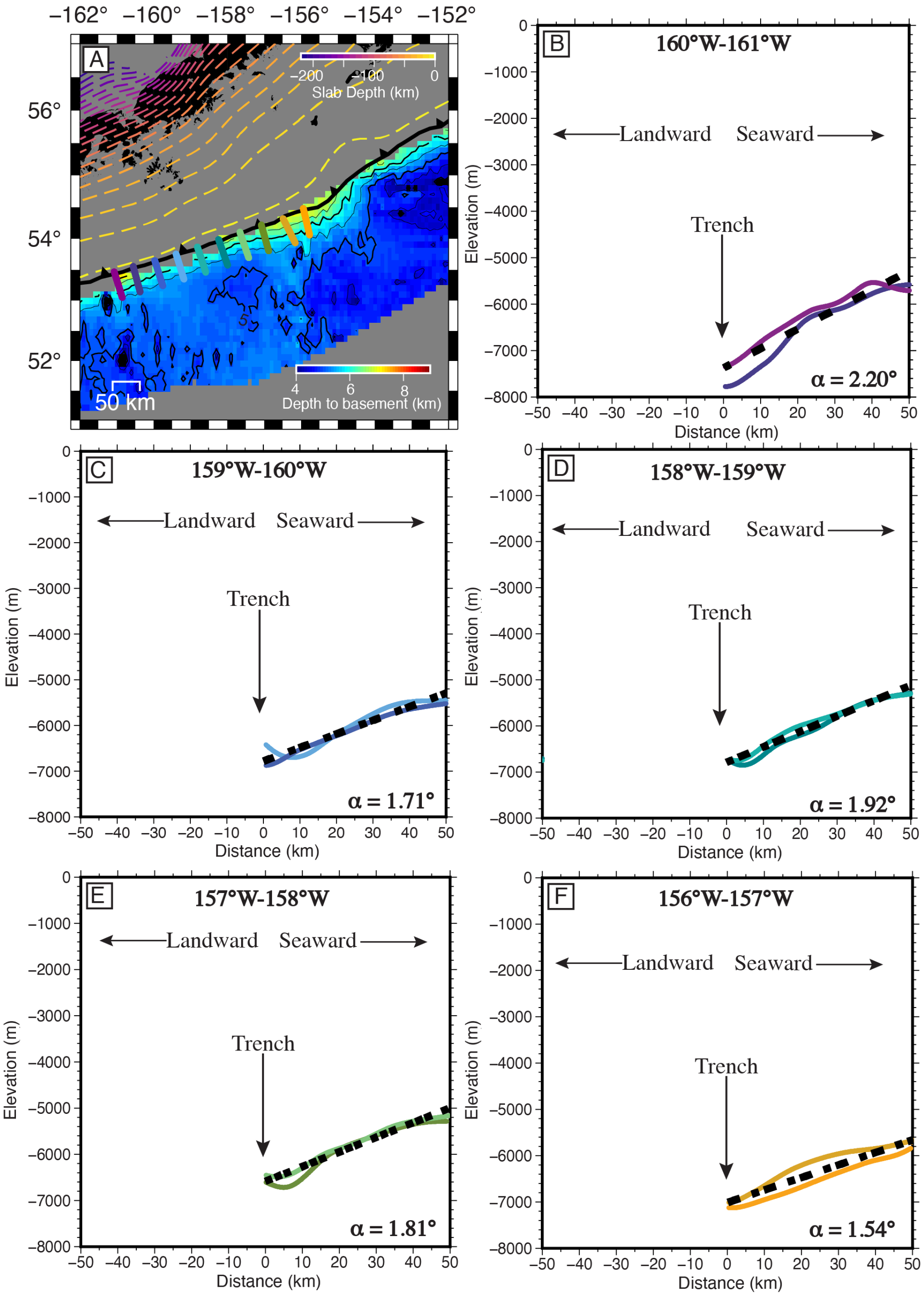

Figure 6: A) Regional map showing the locations of profiles used to estimate outer rise dip outboard of the trench and grid of depth to basement based on bathymetry data (Fig. 1) and sediment thickness (Fig. 4). Colored trench-perpendicular profiles match those in B-F. B-F). Linear regressions (black dashed lines) through two bathymetric profiles (colored lines, see panel A for location) ~0.5 degrees apart. Dip angles (alpha) for each longitudinal bin labeled on plot. For comparison, we also estimated dip of the incoming plate at the seafloor (Fig. S-6), which also shows a general westward increase in incoming plate dip.

4 Results

We map 255 bending-related faults offshore of the Alaska Peninsula between longitudes 161°W and 155°W. Bending faulting is observed progressively farther from the trench outboard of the eastern Semidi segment compared to outboard the western Shumagin segment. In the western part of the study area (west of 158°W), most bending faults are concentrated within 50 km of the trench, but farther east faults are observed up to 75 km from trench (Figs. 2, S-3). We do not observe any active bending-faults east of 156°W in the newly acquired bathymetry data; all the potential structures that can be mapped here are oriented roughly N-S (Fig. 2B) and likely represent differential compaction over relict abyssal-hill spreading faults or associated structures.

Individual mapped faults have lengths of ~10-20 km, with a maximum length of 48 km, are spaced ~ 3 km apart, and have maximum estimated throws of up to 423 m. Fault length varies along the trench, with average lengths of 15.6 km, 13.9 km, 20.6 km, 19.7 km, and 10.6 km, in 1º bins from 161ºW to 156ºW. There are similar numbers of faults dipping toward the trench and away from the trench. However, faults that dip trenchward generally exhibit larger throws than those dipping seaward (Fig. S-3). Cumulative fault throw summed across all mapped faults increases markedly from east to west, with the eastern portion having both fewer total number of faults and smaller estimated fault throws than the west (Fig. 7).

A comparison of bending fault azimuths with the orientations of the trench and magnetic anomalies shows that bending faults generally parallel pre-existing structures (Fig. 3). Bending-related faults in our study area primarily have strike azimuths between 80-100° (Fig. 3). West of 157.5ºW, magnetic anomalies parallel inferred abyssal-hill faults, which dominantly strike E-W (azimuths of 80-90°). Here faults strike 10-20° oblique to the trench axis which has a relatively uniform azimuth of ~70° (Figs. 2C, 3). Between 157.5 and 156ºW, magnetic anomalies are less continuous and have more variable orientations, including some that strike ENE-WSW, nearly parallel to the trench axis. East of 156ºW, magnetic anomalies strike ~N-S and no bending faults are observed.

There are two key areas where fault strikes are not subparallel to magnetic anomaly trends. The first is at ~159.25-160°W, where bending fault strikes show one dominant trend centered at ~85° and a broad secondary trend ranging from ~35-80°. This area also contains small mounds (Fig. 2B) that we tentatively interpret as petit spot volcanic constructs due to their morphological similarity to petit spot volcanoes found at other subduction zones, such as the Japan trench (Hirano, 2011; Hirano et al., 2006). The second is located between 156-157ºW where fault strike azimuths span a wide range from ~35-100° (Fig. 3). This region is just west of the magnetic anomaly trends rotating from N-S to ENE-WSW. In both of these regions, fault lengths are generally shorter than in surrounding areas.

The dip of the incoming plate at the top of basement near the trench gradually increases from east to west, from a dip angle of ~1.6° seaward of the eastern portion of the Semidi segment between longitudes 156°W and 157°W, to 2.2° seaward of the westernmost part of the Shumagin Gap between longitudes 160°W and 161°W (Fig. 6). This increase in dip of the top of basement near the trench mirrors the dip at the seafloor in the outer rise (Fig. S-6) and the gradual increase in slab dip and curvature observed at greater depths (e.g., Fig. 1; Hayes et al., 2018; Kuehn, 2019).

Sediment thickness also varies along strike, with the thinnest sediment cover offshore of the Shumagin Gap (~400 m) in the western portion of the study area and the thickest sediment cover (~1100 m) offshore of the Semidi segment in the east (Fig. 4). The increase in total sediment thickness between ~155°W and 157°W can largely be attributed to the precense of the Oligocene-Miocene aged terrestrial Zodiac fan, contributin >500 m of pelagic sediment and terrigenous turbidites (Creager et al., 1973; Stevenson et al., 1983; von Huene et al., 2012). This fan formed off the coast of the Pacific Northwest of the United States (off the coast of present-day Washington and Oregon) and was transported on the Pacific plate through its northward migration over the last 32-40 Ma (Stevenson et al., 1983). Sediment thickness varies from an average of 250 m to a maximim thickness of ~1,600 m. The thickest sediments are observed in the central part of the Zodiac fan and near the head of the fan, and sediment thickness decreases towards the edges of the fan (Stevenson et al., 1983). Smaller-scale variations may be caused by filling in irregular seafloor topography. For example, this may occur in the eastern part of the study area where oceanic crust was accreted at intermediate spreading rates and is rougher than in the west. The area of thin sediments east of the study area between ~152-148ºW occurs in the area of the Patton Murray seamount chain (Fig. 4). Pelagic sediments and terrigenous Zodiac fan sediments were deposited on the oceanic plate prior to bending and are thus expected to be offset by these younger bending faults.

We also quantify the thickness of trench-fill sediments, as these sediments are deposited during bending and subduction and thus have the greatest potential to mask bending faulting at the seafloor. Trench fill sediments are deposited primarily by along-trench transport (von Huene et al., 2012). Although trench fill sediments are up to 1.5 km thick, they are generally confined to a narrow (~10-20 km) region near the trench, and bending faulting extends upwards of 50-70 km from the trench (Figs. 4, 5).

5 Discussion

5.1 Estimating bending fault throw and the impact of sediment cover on fault mapping

Cumulative bending-related fault throw is greatest outboard of the western Shumagin Gap between 159-161ºW and decreases eastward from 158ºW to 156ºW; east of 156ºW outboard of the eastern Semidi region, no bending faulting is apparent in the bathymetry or seismic data (Figs. 2, 5, 7). Faults observed in the seismic data east of 156ºW in the igneous crust are oriented roughly N-S (Fig 2.) and most likely features created during crust formation. The crust in this region formed at slower spreading rates than crust to the west (Engebretson et al., 1985), creating a rougher crust surface (Buck et al., 2005; Buck & Poliakov, 1998; Carbotte & Macdonald, 1994). Possible faulting that may exist in the sediment cover offshore of the eastern Semidi segment (Fig 5B) is therefore not likely caused by active faulting and may instead be caused by differential compaction of sediments over a fractured crust surface (Carvers, 1968). These results are consistent with previous seismic reflection imaging of bending faults in widely spaced seismic reflection profiles and with a documented westward increase in the frequency of outer rise earthquakes (Matulka et al., 2022; Shillington et al., 2015).

One possible contribution to the apparent eastward decrease in cumulative fault throw at the seafloor could be masking by sediments, which increases in thickness to the east (e.g., Shillington et al., 2015; Li et al., 2018, von Huene et al., 2012, Fig. 4). However, the Zodiac fan and other pelagic sediments on the oceanic crust are older than active bending faults in the present-day outer rise. Active faulting due to plate bending should, therefore, cut these older sediments, and fault scarps should still be evident on the seafloor even in the region covered by the fan. Quaternary trench fill sediments, on the other hand, were deposited during bending faulting and thus could mask the seafloor expressions of these faults, but we find that these sediments are confined to a narrow (~10-20 km) region near the trench and vary significantly in thickness along strike from existing seismic data, and thus cannot account for the systematic eastward decrease in bending faulting we observe in bathymetry data.

5.2 Controls on bending faulting strike orientations and throw

New constraints on bending faulting from this study offer the opportunity to examine controls on the orientations of bending faults and along-strike variations in cumulative outer rise fault throws.

5.2.1 Bending fault strike orientations

Previous analyses on controls on bending fault formation (e.g., Billen et al., 2007; Masson, 1991) found that abyssal-hill faults are reactivated when they are oriented <25-30º of the trench and bending forms new faults when the angle between the spreading fabric and trench is >25-30°. Bending-related faults that reactivate pre-existing abyssal hill faults are expected to strike parallel to magnetic anomalies generated by seafloor spreading, and newly formed faults are expected to strike parallel the trench axis. In our study area, most bending faults strike parallel to magnetic anomalies suggesting that they formed by reactivation (Fig. 3), consistent with the previous studies of this area (Masson, 1991; Shillington et al., 2015). This is also consistent with observations at other subduction zones where pre-existing structures are near parallel to the trench, including the western Aleutians (Masson, 1991; Mortera-Gutiérrez et al., 2003), offshore Nicaragua (Ranero et al., 2003; Van Avendonk et al., 2011), and in the Kuril subduction zone (Fujie et al., 2018; Kobayashi et al., 1998).

The average throws (~300 m) and average spacing (~3 km) of bending faults offshore of the Alaska Peninsula are similar to the characteristics of bending faults in other locations where bend faulting occurs primarily by reactivation of abyssal hill faults (e.g., Fujie et al., 2018; Ranero et al., 2003). Fault spacing is ~5 km at the Kuril trench (Fujie et al., 2018) and ~2 km at the Middle America Trench (Faccenda et al., 2009; Ranero et al., 2003) where abyssal-hill faults are reactivated. When new bending faults form and cut across pre-existing fabrics, they often have larger throws and are more widely spaced compared to reactivated faults, as is observed at the Chilean and northern Japan trenches (e.g., Fujie et al., 2018; Geersen et al., 2018). In the eastern part of our study area (<156ºW), where pre-existing structures are oblique to the trench, bending faults are not observed (Fig. 8). We discuss a possible explanation for the absence of bending faulting in the east in Section 5.2.2.

There are two regions within our study area (156-157ºW and 159-160ºW, Fig 3) that exhibit bending faults with a broader range of strikes that do not parallel magnetic anomalies. The region between 156-157ºW occurs north of the relict ridge-ridge-ridge triple junction and thus may have more complicated pre-existing structures. Complex and evolving abyssal-hill faulting is observed near modern ridge-ridge-ridge triple junctions and other areas of spreading changes (Smith et al., 2011), and the same may have been true in this area. Large topographiuc features such as the structure near 156ºW could locally influence stress state and fault orientation (Geersen et al., 2022). However, we assert that complex variations in pre-existing structures are the primary controlling factors between between 156-157ºW. We discuss the region between 159-160ºW in Section 5.3

5.2.2 Cumulative bending-related fault throw

We observe a significant westward increase in the summed throw of all mapped faults within 0.5º bins (Fig. 7). Slab curvature is thought to be a primary control on the amount of slip on bending faults, where higher degrees of slab bending are expected to be associated with larger magnitudes of cumulative fault slip (Faccenda, 2014). In our study area, the bending angle of the incoming plate estimated from the dip of the top of basement crust in seismic reflection data (Fig. 6) steepens to the west, consistent with westward steepening of slab dip and increase in slab curvature at depth (Fig. 1; Buffett & Heuret, 2011; Hayes et al., 2018; Kuehn, 2019). This correlation suggests that the increase in slab dip could contribute the westward increase in cumulative bending faulting. However, given the relatively modest changes in slab curvature along-strike of ~1º over five degrees of longitude, it is surprising that we observe such a large and abrupt along-strike change in the amount of bending faulting: from no discernable bending faulting east of 156ºW to significant bending faulting between 159-161ºW. Therefore, while changes in slab dip likely contribute to the westward increase in observed cumulative bending faulting, other factors appear necessary to explain the relatively abrupt along-strike change in summed fault throws.

An abrupt change in pre-existing fabric in the subducting plate provides one possible explanation for the abrupt observed change in observed summed fault throws between 156-158ºW. Magnetic anomaly patterns suggest that pre-existing structures west of 158ºW are E-W striking and thus near parallel to the trench and favorable for reactivation, while east of 156ºW they strike ~N-S, up to 70º oblique to the trench (Fig. 2C; Shillington et al., 2015), unfavorable for reactivation. In the transition between these domains (156-158ºW), the near-trench magnetic anomalies generally trend E-W, but they become weaker and less linear as one moves east, perhaps due to proximity to the relict triple junction directly to the south, and the transition to orthogonal (N-S) fossil ridge orientation directly to the east as discussed above (Fig. 2C, Engebretson et al., 1985; Lonsdale, 1988). Abundant faults are observed within this transition (Fig. 3), but their cumulative slip is relatively modest (Fig. 7), perhaps due to the complicated spreading fabric.

Reactivation of remnant structures, which are estimated to be ~30% weaker than the surrounding crust (Billen et al., 2007), could allow extensional strain in the upper lithosphere to be accommodated by faulting west of ~158ºW. In contrast, to the east, where favorably oriented weaknesses diminish and eventually disappear, bending stresses may not exceed the yield strength of the upper lithosphere and thus limited faulting occurs. This interpretation implies that bending stresses alone may be insufficient to promote the formation of outer rise faults in the oceanic lithosphere in locations that have modest slab dip and that lack inherited weaknesses. For comparison, slab dip is significantly steeper (by ~2º) in other subduction zones where new bending faults form without reactivating pre-existing structures (e.g., Japan and Chilean subduction zones (Fujie et al., 2013; Nishikawa & Ide, 2015; Ranero et al., 2005).

It has been hypothesized that weakening of the oceanic plate by faulting at the outer rise and associated hydration and serpentinization could provide a positive feedback to induce additional slab bending and outer rise faulting (Billen & Gurnis, 2005; Contreras-Reyes & Osses, 2010; Faccenda et al., 2012; Hyndman & Peacock, 2003; Ranero et al., 2003). In Alaska, favorably oriented pre-existing structures may be important for this feedback to initiate as they allow faulting and hydration even at modest bending angles.

The long wavelength over which slab dip steepens along the Alaska subduction zone primarily reflects the transition from flat-slab subduction in the Gulf of Alaska to the east (Davis & Plafker, 1986; Petersen et al., 2021) to normal ocean-ocean plate subduction to the west. The rapid transition in bending-related faulting observed in our region may induce an additional short-wavelength transition in plate weakening that may enhance westward slab steepening. A westward reduction in plate strength at the outer-trench slope is also consistent with a decrease in the distance from the trench where bending faulting initiates: up to ~75 km from trench at ~157ºW but confined to <50 km from trench farther west (Fig. 2). Bending and faulting are expected to occur over larger wavelengths for stronger plates. Similar relationships between pre-existing structures, outer rise faulting, and slab bending angles are observed in the Middle America subduction zone offshore Costa Rica and Nicaragua (Ranero et al., 2003).

In summary, we propose that the combination of along-strike changes in slab dip and the orientation of pre-existing structures with respect to the trench best explains a relatively abrupt along-strike change in the amount of faulting. The steeper slab dips and favorably oriented pre-existing structures, which are weaker than the surrounding crust, allow pervasive bending faulting in the west where larger faults, with greater throws form. In the east, bending stresses associated with modest slab bending may not exceed the yield strength of the lithosphere, and pre-existing structures are highly oblique to the trench, so limited faulting is observed. Feedbacks between pre-existing structures, bending faulting, and plate weakening due to bending faulting may further promote faulting in the west (e.g., Billen & Gurnis, 2005; Contreras-Reyes & Osses, 2010).

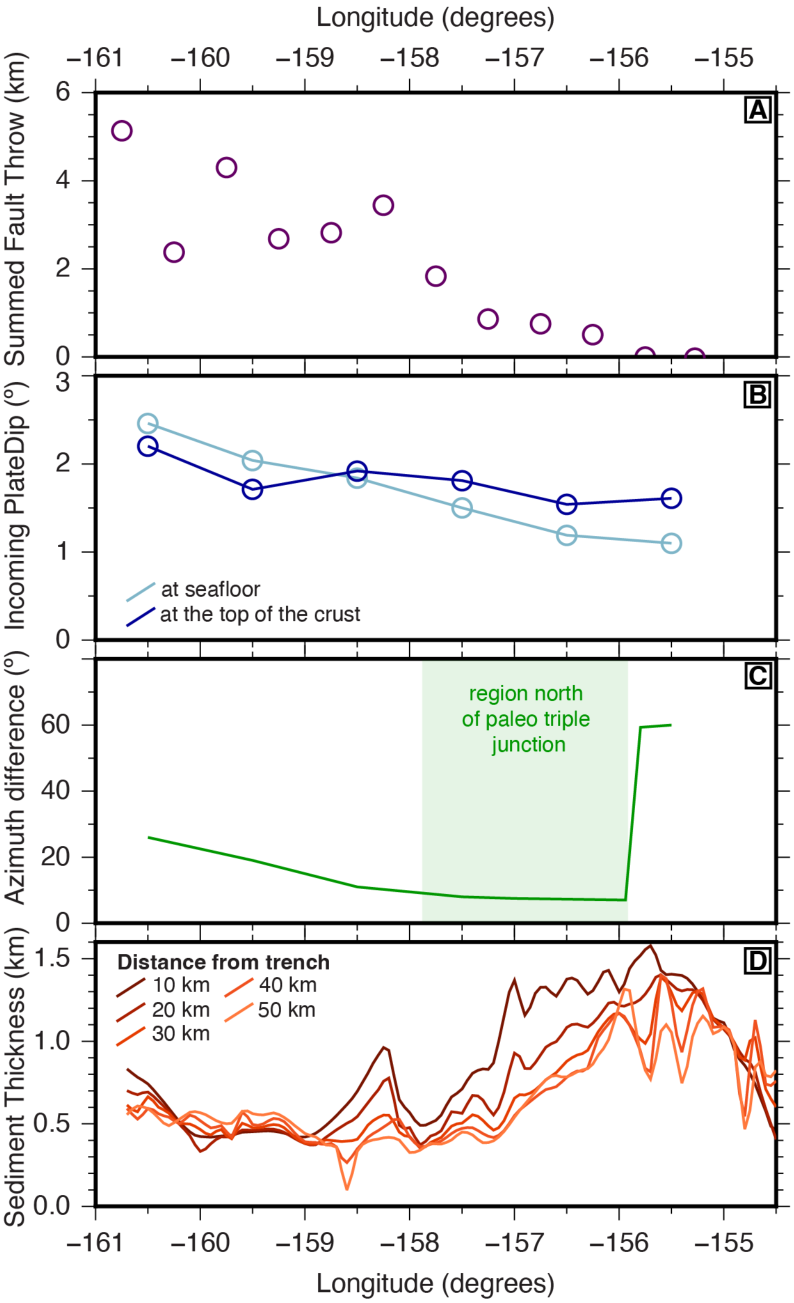

Figure 7: Along strike variations in a) summed maximum throws on bending faults within 0.5º-wide bins; b) dip of the subducting plate at the outer rise, estimated from bathymetric seafloor slope (light blue, Fig. S6) and from the dip of the top of the crust based on a structure contour map of the base of incoming plate sediments (dark blue, Fig. 6); c) difference between the expected strike of pre-existing structures from magnetic anomalies and the trench; d) incoming plate sediment thickness on the incoming plate at distances of 10-50 km from the trench.

5.3 Complex faulting and possible linkage to October 2022 M7.6 intraplate event

Between ~159-160ºW, we observe an area of relatively complex bending-related faulting (Figs. 3, 9). Outside of this area, fault orientations generally exhibit a single, dominant peak in azimuth centered around the average trend of magnetic anomalies (~85-90º). Within the complex zone, a peak is still observed at ~85°, but with an additional broad plateau with abundant faulting spanning orientations between 35-80° (Fig. 3). At ~159.25°W, we also observe a series of features that we interpret as small volcanic constructs (Fig. 8). Similar features are recognized in the outer rises of other subduction zones (e.g., Japan trench; Fujie et al., 2020; Hirano, 2011; Hirano et al., 2006) and categorized as petit-spot magmatism. Off Japan, petit-spot volcanic provinces do not geochemically resemble mid-ocean ridge melts or occur near hotspot centers and are thus hypothesized to be caused by partial melting of the asthenosphere induced by plate bending and fracturing (Hirano et al., 2006).

The complex faulting in this region suggests comparable complexity in the pre-existing structures or stress state of the incoming plate in this region. Magnetic anomalies are relatively continuous through this region, and thus there is no evidence for the former here. Given the short length scales associated with the complexity, we require a mechanism that can produce a relatively abrupt changes in plate stress. Geodetic observations indicate a relatively abrupt change in megathrust coupling between the Shumagin Gap (~159-162ºW) and the Semidi segment (~155-159ºW; Drooff & Freymueller, 2021; Xiao et al., 2021), with a transition approximately coincident with the region of complex faulting. Along-strike variations in megathrust coupling and coseismic slip have been invoked to explain differences in incoming plate seismicity in many subduction zones (e.g., Christensen & Ruff, 1988; Emry et al., 2014), and it is possible that changes in coupling could also cause complexities in stress in the incoming plate over long time periods and thus explain the complex bending-related faulting we observe.

Complex patterns of stress and faulting within the incoming plate could also promote the generation of small amount of melt and intraplate volcanism. Valentine & Hirano (2010) and Hirano (2011) suggest that localization of tensional tectonic forces can enable partial melting in the lower lithosphere, producing intraplate volcanic provinces. Thus, varied stresses in the downgoing plate caused by differential coupling of the slab interface may localize tectonic stresses in the downgoing plate such that melts are generated and accumulate in this transition region and extrude as petit-spot volcanic features.

The region of complex faulting and petit-spot volcanism that we observe between 159-160ºW lies updip from the Oct 2020 M7.6 intraplate event, raising the possibility that they could have related origins. Two causes have been proposed for this enigmatic earthquake, which appears to have ruptured a steep fault in the subducting plate that strikes ~15º and thus orthogonal to the trench: 1) reactivation of remnant spreading features produced at the Kula-Resurrection ridge, which is now subducted (Fuston & Wu, 2020; Jiang et al., 2022); 2) accumulated shear stresses caused by lateral variability in slab dip and coupling (Herman & Furlong, 2021). In the first case, the 2020 M7.6 event is modeled as right-lateral strike-slip motion on a N-S striking fault dipping steeply to the east (Jiang et al., 2020), with slip distribution and associated aftershocks extending to within 30 km laterally from the zone of complex faulting. If this event reactivates hypothesized pre-existing Kula-Resurrection fabric just north of the trench (Fuston and Wu, 2020), then it is plausible that persistent slip on this feature has induced static stress changes in the incoming plate just up-dip of the fault tip (Yang et al., 2023) that are sufficient to perturb the bending stresses and associated fault orientations. In the second case, accumulated stresses in the subducting plate arising from lateral variability in coupling between the Shumagin Gap and Semidi segment could explain both the occurrence of the M7.6 intraplate earthquake (Herman & Furlong, 2021) and the complexities we observe bending-related faulting patterns outboard of the trench. Although more work is needed to evaluate the influence of changes in megathrust coupling on long-term deformation in the incoming plate, the spatial proximity of the earthquake and complex faulting imply a common origin.

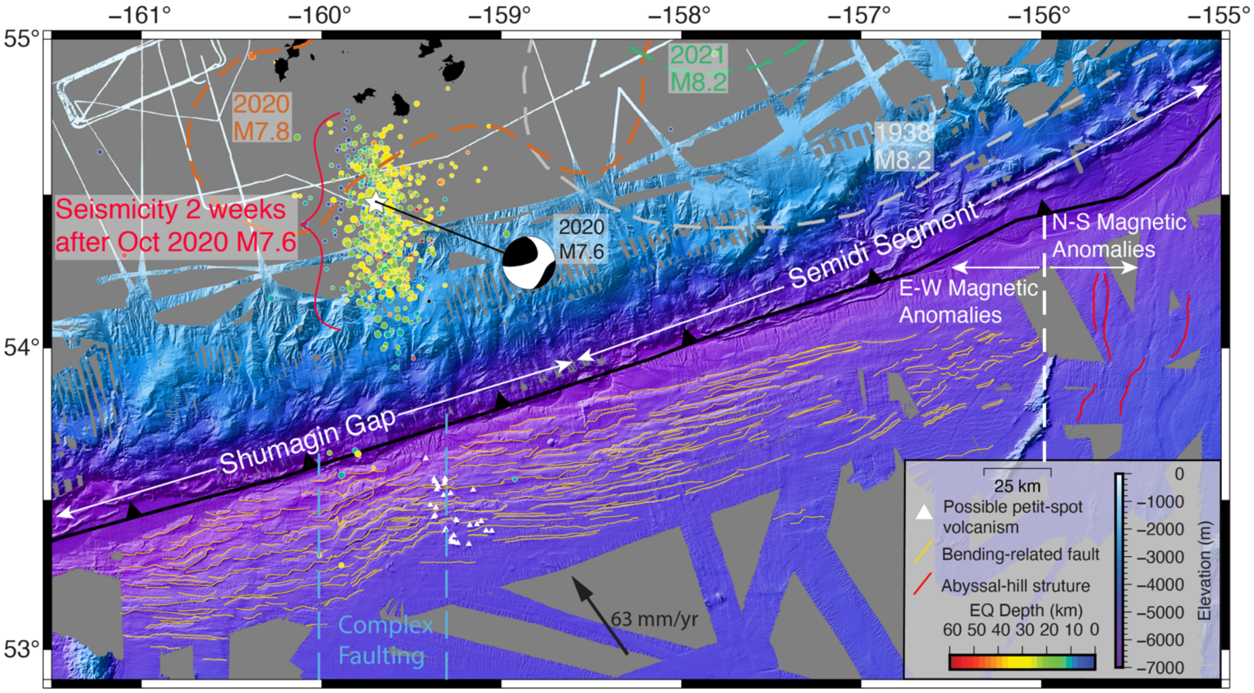

Figure 8: Bathymetric map of bending-related faulting (yellow lines) with abyssal-hill structures (red lines). Also shown is the CMT solution (Dziewonski et al., 1981; Ekström et al., 2012) for the Oct 2020 M7.6 intraplate event and earthquakes two weeks after the M7.6 (points colored by depth; from the Alaska Earthquake Information Center). Highlighted between the dashed blue lines is an area of complex bending faulting between ~159.25-160°W, which lies immediately updip of the 2020 M7.6 intraplate event. Interpreted petit-spot volcanism (white triangles) at ~159.25°W occurs on the eastern edge of the region of complex faulting. Large megathrust rupture patches are shown on the overriding plate colored the same as previous figures.

5.4 Implications for hydration

One major importance of bending-related faulting is its role in allowing ingress of seawater and hydration of the crust and upper mantle of the incoming plate (Cai et al., 2018; Faccenda, 2014; Faccenda et al., 2009; Grevemeyer et al., 2018; Ivandic et al., 2008; Korenaga, 2017; Nishikawa & Ide, 2015; Peacock, 2001; Ranero et al., 2003; Shillington et al., 2015). Extensional faults on the incoming plate are thought to act as conduits for seawater to percolate several kilometers through the crust and into the upper mantle of the incoming plate. The water may reside as fluid-filled cracks in the crust and upper mantle (Miller et al., 2021), as well as react with the peridotites to form serpentinite (Carlson & Miller, 2003; Faccenda, 2014; Faccenda et al., 2009; Grevemeyer et al., 2018; Korenaga, 2017; Peacock, 2001; Ranero et al., 2003). Seismic velocity models from subduction zones around the globe show the reduced velocities in the crust and upper mantle of the subducting plate near the trench, which are interpreted to represent the presence of hydrous minerals and or fluid-filled cracks (Cai et al., 2018; Contreras-Reyes et al., 2007, 2011; Fujie et al., 2018; Ivandic et al., 2008; Shillington et al., 2015; Van Avendonk et al., 2011).

P-wave velocity models in the study area exhibit a more pronounced reduction in seismic velocity in the upper mantle of the incoming plate outboard of the Shumagin Gap (western portion of the study area; west of ~157°W) than in the Semidi segment (eastern portion of the study area; east of ~157°W), suggesting greater hydration in the west (Shillington et al., 2015). Likewise, high-resolution P-wave models from streamer tomography also show a reduction in velocity in the upper crust off the Shumagin Gap, interpreted to arise from a combination of faulting and alteration (Acquisto et al., 2022).

The combination of preferentially oriented pre-existing structures and an increase in slab dip outboard of the Shumagin Gap (west of ~157°W) promote more bending faulting and are thus expected to produce increasing hydration of the incoming lithosphere, in comparison to the region outboard of the Semidi segment (east of ~157°W) where the number and size of bending faulting is lower, A westward increase in hydration can be inferred from the westward increase in number of faults and larger fault throws and is consistent with observations of a double-seismic zone in the downgoing plate in the Shumagin Gap (Wei et al., 2021), prominent conductors at depth in magnetotelluric data (Cordell et al., 2023), and geochemical signatures consistent with fluids in arc volcanism in the western Shumagin Gap (Wei et al., 2021).

Faults to the west of our study area also appear to have more irregular fault orientations (Figs. 2B & 3) and may form interconnected fault networks as they grow and merge near the trench, thus creating a larger and more pervasive damaged zone. This interconnected fault network to the west could also promote increased hydration.

5.5 Implications for plate boundary properties

Geodetic studies of the Alaska Peninsula show that the western Shumagin Gap is <30% coupled, whereas the eastern Semidi segment is almost entirely locked (Drooff & Freymueller, 2021; Li & Freymueller, 2018). Changes in subduction zone inputs could influence changes in coupling here (Shillington et al., 2015). Westward increases in the total number and throws of bending-related faults on the incoming plate, combined with the westward decrease in sediment thickness, can influence the heterogeneity of the megathrust interface once subducted. Possible petit-spot features at ~159.25°W may also locally contribute to a rougher plate interface in the western part of our study area. Rough seafloor is proposed to promote creeping of the megathrust interface and numerous small to medium (< M7.5) events (Wang & Bilek, 2014) and potentially contribute to slow slip events (e.g., Saffer & Wallace, 2015). Higher degrees of bending faulting to the west are also expected to result in greater hydration of the crust and upper mantle, stored in hydrous minerals or as free water. Dehydration and migration of fluids at depth could also influence megathrust properties and behavior (e.g., Cordell et al., 2023; Saffer & Tobin, 2011; Saffer & Wallace, 2015). Thus, increased bending faulting and thinner sediment cover on the incoming plate in the western part of the study area may lead to a heterogeneous and fluid-rich megathrust interface and promote creep. The lack of bending faulting and larger amounts of sediment entering the subduction zone in the eastern Semidi segment (Li et al., 2018) could contribute to greater megathrust homogeneity. At shallow depths, the thicker subducted sediments in the Semidi segment appear to be overpressured (Li et al., 2018) and may contribute to observed aseismic slip (e.g., He et al., 2023). At greater depths, thicker subducting sediments could contribute to a relatively homogenous plate boundary, allowing for increased locking and propensity to rupture in earthquakes in the eastern portion of our study area (Li et al., 2018; Ruff, 1989).

On the other hand, thinner sediment and rougher seafloor subducting in the Shumagin segment may promote shallow seismic slip and tsunamigenesis (Bécel et al., 2017). These properties are commonly associated with the incoming plate in subduction zones with shallow, tsunamigenic earthquakes, including tsunami earthquakes (Polet & Kanamori, 2000). Subduction zones with low coupling can host infrequent tsunamigenic earthquakes. For example, the 1946 M8.6

tsunami earthquake ruptured a weakly coupled region to the west of our study area (López & Okal, 2006). Bécel et al. (2017) proposed that the properties of the Shumagin sector, including the rough seafloor and paucity of sediments, may make it prone to tsunamigenic shallow slip when infrequent large earthquake rupture into this weakly coupled segment as may have occurred in 1788 (Davies et al., 1981).

We acknowledge that there are uncertainties associated with projecting features observed outboard of the subduction zone to seismogenic depths. The position of features at depth is influenced by slab geometry and convergence direction (Harmon et al., 2019). In the study area, there are significant uncertainties in the continuation of the Zodiac fan at depth (von Huene et al., 2012), and competing reconstructions for the spreading history in this region predict different configurations of pre-existing structures at depth (e.g., Fuston & Wu, 2020). Nonetheless, the correlations between incoming plate properties, changes in locking and seismicity at a range of depths, and arc lava chemistry imply that subduction zone inputs contribute to patterns of plate boundary behavior (Shillington et al., 2015; Wei et al, 2021).

6 Conclusions

Analysis of new high-resolution bathymetry data collected outboard of the Shumagin Gap and Semidi segment provide new insights into controls on formation and patterns of bending-related faulting in the outer-rise of the incoming Pacific plate.

1) Bending-related faults strike dominantly parallel to magnetic anomalies, indicating that bending primarily reactivates relict abyssal-hill faults originating at oceanic plate formation. The

angle between magnetic anomalies and the trench controls bending fault strike, where reactivated faults parallel magnetic anomalies and newly formed faults parallel the trench.

2) The plate bends more steeply to the west in the Shumagin Gap region, where observed faulting is more extensive and where larger faults, with greater throw, form. These observations suggest that increased bending of the downgoing plate is likely one contributing factor to the westward increase in summed scarp heights. However, feedbacks between pre-existing structures, slab weakening, and bending and faulting appear necessary to explain the relatively abrupt along-strike changes in the amount of bend faulting.

3) The subducting plate updip of the M7.6 intraplate earthquake (between 159-160ºW) exhibits relatively complex bending faulting and petit spot volcanism. Variations in coupling and slab dip could contribute to both bending faulting patterns and the M7.6 earthquake here.

4) The westward increase in bending faulting has important implications for incoming plate weaknesses and the ability for bending-faulting to pervasively hydrate the incoming plate at the western Shumagin Gap.

5) Thin sediment cover and pervasive bending-related faulting on the incoming plate outboard of the western Shumagin Gap promotes a heterogeneous, fluid rich plate interface and creeping megathrust behavior at depth. Thick sediment cover and nearly absent bending-related faulting on the incoming plate outboard of the eastern Semidi segment promotes a homogeneous megathrust, contributing to recurring great earthquakes.

Acknowledgements

We gratefully acknowledge the scientists and ship crews of the R/V *Langseth* and R/V *Sikuliaq* responsible for the collection of bathymetry data during the Alaska Amphibious Community

Seismic Experiment (AACSE). This work was supported by NSF-OCE-2026676 to NAU and NSF-OCE- 2025969 to Washington University. Freely available Generic Mapping Tools (GMT) and OpendTect software were used in data analysis and display. We thank two anonymous reviewers and the associate editor for constructive comments that imporoved the manuscript.

Open Research

All of the data used in this paper are opening available. Bathymetry data can be accessed through the Marine Geoscience Data System (https://www.marine-geo.org/index.php) and is searchable by expedition code (R/V Sikuliaq: SKQ201811S, SKQ201816S, SKQ201918S R/V Langseth: MGL1903, MGL1907). Seismic reflection data from ALEUT (https://www.marine-geo.org/tools/entry/MGL1110) and AACSE (https://www.marine-geo.org/tools/entry/MGL1903) are also available through the MGDS, and USGS reflection data are available from NAMSS (https://walrus.wr.usgs.gov/namss/).

References

Abers, G. A. (1992). Relationship between shallow-and-intermediate depth seismicity in the eastern Aleutian subduction zone. *Physics of the Earth and Planetary Interiors*, *19*, 2019–2022. http://linkinghub.elsevier.com/retrieve/pii/S0031920104001657

Acquisto, T., Bécel, A., Singh, S. C., & Carton, H. (2022). Evidence of strong upper oceanic crustal hydration outboard the Alaskan and Sumatran subduction zones. *Journal of Geophysical Research: Solid Earth*, *127*, e2022JB024751.

Bankey, V., Cuevas, A., Daniels, D. L., Finn, C. A., Hernandez, I., Hill, P. L., Kucks, R., Miles, W., Pilkington, M., Roberts, C., Roest, W., Rystrom, V., Shearer, S., Snyder, S. L., Sweeney, R. E., & Velez, J. (2002). *Magnetic anomaly map of North America*. https://doi.org/10.3133/70211067

Barcheck, G., Abers, G. A., Adams, A. N., Bécel, A., Collins, J., Gaherty, J. B., Haeussler, P. J., Li, Z., Moore, G., Onyango, E., Roland, E., Sampson, D. E., Schwartz, S. Y., Sheehan, A. F., Shillington, D. J., Shore, P. J., Webb, S., Wiens, D. A., & Worthington, L. L. (2020). The Alaska Amphibious Community Seismic Experiment. [Dataset]. *Seismological Research Letters*, *91*(6), 3054–3063. https://doi.org/10.1785/0220200189

Bassett, D., & Watts, A. B. (2015). Gravity anomalies, crustal structure, and seismicity at subduction zones: 1. Seafloor roughness and subducting relief. *Geochemistry Geophysics Geosystems*, *16*, 1508–1540. https://doi.org/10.1002/2014GC005684

Bécel, A., Sheehan, A., Foster, D., Myers, E., Haeussler, P., Abers, G., Adams, A., Roland, E., Schwartz, S., Shillington, D., Wiens, D., Webb, S., & L. Worthington. (2019).

Multi-Channel Seismic Shot Data from the Alaska-Aleutians area acquired during Langseth cruise MGL1903. In *IEDA*. https://doi.org/10.1594/IEDA/324793

Bécel, A., Shillington, D. J., Delescluse, M., Nedimović, M. R., Abers, G. A., Saffer, D. M., Webb, S. C., Keranen, K. M., Roche, P. H., Li, J., & Kuehn, H. (2017). Tsunamigenic structures in a creeping section of the Alaska subduction zone. *Nature Geoscience*, *10*(8), 609–613. https://doi.org/10.1038/NGEO2990

Bécel, A., Shillington, D. J., Nedimović, M. R., Webb, S. C., & Kuehn, H. (2015). Origin of dipping structures in fast-spreading oceanic lower crust offshore Alaska imaged by multichannel seismic data. *Earth and Planetary Science Letters*, *424*, 26–37. https://doi.org/10.1016/j.epsl.2015.05.016

Billen, M. I., & Gurnis, M. (2005). Constraints on subducting plate strength within the Kermadec trench. *Journal of Geophysical Research: Solid Earth*, *110*(5), 1–18. https://doi.org/10.1029/2004JB003308

Bodine, J. H., & Watts, A. B. (1979). On lithospheric flexure seaward of the Bonin and Mariana trenches. *Earth and Planetary Science Letters*, *43*, 132–148.

Boneh, Y., Schottenfels, E., Kwong, K., van Zelst, I., Tong, X., Eimer, M., Miller, M. S., Moresi, L., Warren, J. M., Wiens, D. A., Billen, M., Naliboff, J., & Zhan, Z. (2019). Intermediate-Depth Earthquakes Controlled by Incoming Plate Hydration Along Bending-Related Faults. *Geophysical Research Letters*, *46*(7), 3688–3697. https://doi.org/10.1029/2018GL081585

Buck, W. R., Lavier, L. L., & Poliakov, A. N. B. (2005). Modes of faulting at mid-ocean ridges. *Nature*, *434*(7034), 719–723. https://doi.org/10.1038/nature03358

Buck, W. R., & Poliakov, A. N. B. (1998). Abyssal hills formed by stretching oceanic lithosphere. *Nature*, *392*, 272–275. https://doi.org/10.1038/246170a0

Buffett, B. A., & Heuret, A. (2011). Curvature of subducted lithosphere from earthquake locations in the Wadati-Benioff zone. *Geochemistry, Geophysics, Geosystems*, *12*(6), Q06010. https://doi.org/10.1029/2011GC003570

Buurman, H., Nye, C. J., West, M. E., & Cameron, C. (2014). Regional controls on volcano seismicity along the Aleutian arc. *Geochemistry, Geophysics, Geosystems*, *15*, 1147–1163. https://doi.org/10.1002/2013GC005101

Cai, C., Wiens, D. A., Shen, W., & Eimer, M. (2018). Water input into the Mariana subduction zone estimated from ocean-bottom seismic data. *Nature*, *563*, 389–392. https://doi.org/10.1038/s41586-018-0655-4

Caldwell, J. G., Haxby, W. F., Karig, D. E., & Turcotte, D. L. (1976). On the applicability of a universal elastic trench profile. *Earth and Planetary Science Letters*, *31*, 239–246.

Canales, J. P., Carbotte, S. M., Nedimovic, M. R., & Carton, H. (2017). Dry Juan de Fuca slab revealed by quantification of water entering Cascadia subduction zone. *Nature Geoscience*, *10*(11), 864–870. https://doi.org/10.1038/NGEO3050

Carbotte, S. M., & Macdonald, K. C. (1994). Comparison of seafloor tectonic fabric at intermediate, fast, and super fast spreading ridges: Influence of spreading rate, plate motions, and ridge segmentation on fault patterns. *Journal of Geophysical Research*, *99*(B7), 13609–13631. https://doi.org/doi:10.1029/93JB02971

Carlson, R. L., & Miller, D. J. (2003). Mantle wedge water contents estimated from seismic velocities in partially serpentinized peridotites. *Geophysical Research Letters*, *30*(5), 12–15. https://doi.org/10.1029/2002gl016600

Carvers, R. E. (1968). Differential Compaction as a Cause of Regional Contemporaneous Fault. *American Association of Petroleum Geologists Bulletin*, *52*(3), 414–419. http://pubs.geoscienceworld.org/aapgbull/article-pdf/52/3/414/4456253/aapg_1968_0052_0003_0414.pdf

Chapple, W. M., & Forsyth, D. W. (1979). Earthquakes and Bending of Plates at Trenches. *Journal of Geophysical Research*, *84*(B12), 6729–6749.

Christensen, D. H., & Ruff, L. J. (1988). Seismic Coupling and Outer Rise Earthquakes. *Journal of Geophysical Research*, *93*(B11), 13,421-13,444. https://doi.org/10.1029/JB093iB11p13421

Contreras-Reyes, E., Grevemeyer, I., Flueh, E. R., Scherwath, M., & Bialas, J. (2008). Effect of trench-outer rise bending-related faulting on seismic Poisson's ratio and mantle anisotropy: A case study offshore of Southern Central Chile. *Geophysical Journal International*, *173*, 142–156. https://doi.org/10.1111/j.1365-246X.2008.03716.x

Contreras-Reyes, E., Grevemeyer, I., Flueh, E. R., Scherwath, M., & Heesemann, M. (2007). Alteration of the subducting oceanic lithosphere at the southern central Chile trench-outer rise. *Geochemistry, Geophysics, Geosystems*, *8*(7), Q07003. https://doi.org/10.1029/2007GC001632

Contreras-Reyes, E., Grevemeyer, I., Watts, A. B., Flueh, E. R., Peirce, C., Moeller, S., & Papenberg, C. (2011). Deep seismic structure of the Tonga subduction zone: Implications for mantle hydration, tectonic erosion, and arc magmatism. *Journal of Geophysical Research*, *116*(10), B10103. https://doi.org/10.1029/2011JB008434

Contreras-Reyes, E., & Osses, A. (2010). Lithospheric flexure modelling seaward of the Chile trench: Implications for oceanic plate weakening in the Trench Outer Rise region. *Geophysical Journal International*, *182*, 97–112. https://doi.org/10.1111/j.1365-246X.2010.04629.x

Cordell, D., Naif, S., Evans, R., Key, K., Constable, S., Shillington, D., & Bécel, A. (2023). Forearc seismogenesis in a weakly coupled subduction zone influenced by slab mantle fluids. *Nature Geoscience*, *16*, 826827. https://doi.org/10.1038/s41561-023-01260-w

Creager, J. S., Scholl, D. W., Boyce, R. E., Echols, R. J., Lee, H. J., Ling, H. Y., Stewart, R. J., Supko, P. R., & Worsley, T. R. (1973). Deep sea drilling project initial reports: site 183. *DSDP*, *19*, 1–19.

Davies, J., Sykes, L., House, L., & Jacob, K. (1981). Shumagin Seismic Gap, Alaska Penninsula: History of Great Earthquakes, Tectonic Setting, and Evidence for High Seismic Potential. *Journal of Geophysical Research*, *86*(B5), 3821–3855. https://doi.org/10.1029/JB086iB05p03821

Davis, A. S., & Plafker, G. (1986). Eocene basalts from the Yakutat terrane: Evidence for the origin of an accreting terrane in southern Alaska. *Geology*, *14*, 963–966.

Drooff, C., & Freymueller, J. T. (2021). New Constraints on Slip Deficit on the Aleutian Megathrust and Inflation at Mt. Veniaminof, Alaska From Repeat GPS Measurements. *Geophysical Research Letters*, *48*, e2020GL091787. https://doi.org/10.1029/2020GL091787

Dziewonski, A. M., Chou, T. A., & Woodhouse, J. H. (1981). Determination of earthquake source parameters from waveform data for studies of global and regional seismicity.

Journal of Geophysical Research, *86*(B4), 2825–2852. https://doi.org/10.1029/JB086iB04p02825

Eimer, M., Wiens, D. A., Cai, C., Lizarralde, D., & Jasperson, H. (2020). Seismicity of the Incoming Plate and Forearc Near the Mariana Trench Recorded by Ocean Bottom Seismographs. *Geochemistry, Geophysics, Geosystems*, *21*(4). https://doi.org/10.1029/2020GC008953

Ekström, G., Nettles, M., & Dziewoński, A. M. (2012). The global CMT project 2004–2010: Centroid-moment tensors for 13,017 earthquakes. *Physics of the Earth and Planetary Interiors*, *200–201*, 1–9. https://doi.org/https://doi.org/10.1016/j.pepi.2012.04.002

Elliot, J. L., Grapenthin, R., Parameswaran, R. M., Xiao, Z., Freymueller, J. T., & Fusso, L. (2022). Cascading rupture of a megathrust. *Science Advances*, *8*, eabm4131.

Emry, E. L., Wiens, D. A., & Garcia-Castellanos, D. (2014). Faulting within the Pacific plate at the Mariana Trench: Implications for plate inerface coupling and subduction of hydrous minerals. *Journal of Geophysical Research, Solid Earth*, *119*, 3076–3095. https://doi.org/10.1002/2013JB010718

Engebretson, D. C., Cox, A., & Gordon, R. G. (1985). Relative Motions Between Oceanic Plates of the Pacific Basin. *Geological Society of America Special Paper*, *206*, 1–60. https://doi.org/10.1029/JB089iB12p10291

Faccenda, M. (2014). Water in the slab: A trilogy. *Tectonophysics*, *614*, 1–30. https://doi.org/10.1016/j.tecto.2013.12.020

Faccenda, M., Gerya, T. V., & Burlini, L. (2009). Deep slab hydration induced by bending-related variations in tectonic pressure. *Nature Geoscience*, *2*, 790–793. https://doi.org/10.1038/ngeo656

Faccenda, M., Gerya, T. V., Mancktelow, N. S., & Moresi, L. (2012). Fluid flow during slab unbending and dehydration: Implications for intermediate-depth seismicity, slab weakening and deep water recycling. *Geochemistry, Geophysics, Geosystems*, *13*, Q01010. https://doi.org/10.1029/2011GC003860

Florez, M. A., & Prieto, G. A. (2019). Controlling Factors of Seismicity and Geometry in Double Seismic Zones. *Geophysical Research Letters*, *46*(8), 4174–4181. https://doi.org/10.1029/2018GL081168

Fujie, G., Kodaira, S., Kaiho, Y., Yamamoto, Y., Takahashi, T., Miura, S., & Yamada, T. (2018). Controlling factor of incoming plate hydration at the north-western Pacific margin. *Nature Communications*, *9*. https://doi.org/10.1038/s41467-018-06320-z

Fujie, G., Kodaira, S., Nakamura, Y., Morgan, J. P., Dannowski, A., Thorwart, M., Grevemeyer, I., & Miura, S. (2020). Spatial variations of incoming sediments at the northeastern Japan arc and their implications for megathrust earthquakes. *Geology*, *48*(6), 614–619. https://doi.org/10.1130/G46757.1

Fujie, G., Kodaira, S., Yamashita, M., Sato, T., Takahashi, T., & Takahashi, N. (2013). Systematic changes in the incoming plate structure at the Kuril trench. *Geophysical Research Letters*, *40*(1), 88–93. https://doi.org/10.1029/2012GL054340

Fuston, S., & Wu, J. (2020). Raising the Resurrection plate from an unfolded-slab plate tectonic reconstruction of northwestern North America since early Cenozoic time.

Bulletin of the Geological Society of America, *133*(5), 1128–1140. https://doi.org/10.1130/B35677.1

Garcia, E. S. M., Sandwell, D. T., & Bassett, D. (2019). Outer trench slope flexure and faulting at Pacific basin subduction zones. *Geophysical Journal International*, *218*, 708–728. https://doi.org/10.1093/gji/ggz155

Geersen, J., Ranero, C. R., Klaucke, I., Behrmann, J. H., Kopp, H., Tréhu, A. M., Contreras-Reyes, E., Barckhausen, U., & Reichert, C. (2018). Active Tectonics of the North Chilean Marine Forearc and Adjacent Oceanic Nazca Plate. *Tectonics*, *37*(11), 4194–4211. https://doi.org/10.1029/2018TC005087

Geersen, J., Sippl, C., & Harmon, N. (2022). Impact of bending-related faulting and oceanic-plate topography on slab hydration and intermediate-depth seismicity. *Geosphere*, *18*(2), 562–584. https://doi.org/10.1130/GES02367.1

Grevemeyer, I., Ranero, C. R., & Ivandic, M. (2018). Structure of oceanic crust and serpentinization at subduction trenches. *Geosphere*, *14*(2), 395–418. https://doi.org/10.1130/GES01537.1

Hacker, B. R. (2008). H2O subduction beyond arcs. *Geochemistry, Geophysics, Geosystems*, *9*(3), Q03001. https://doi.org/10.1029/2007GC001707

Harmon, N., Rychert, C., Collier, J., Henstock, T., Van Hunen, J., & Wilkinson, J. J. (2019). Mapping geologic features onto subducted slabs. *Geophysical Journal International*, *219*(2), 725–733. https://doi.org/10.1093/gji/ggz290

Hasegawa, A., & Nakajima, J. (2017). Seismic imaging of slab metamorphism and genesis of intermediate-depth intraslab earthquakes. *Progress in Earth and Planetary Science*, *4*. https://doi.org/10.1186/s40645-017-0126-9

Hayes, G. P., Moore, G. L., Portner, D. E., Hearne, M., Flamme, H., Furtney, M., & Smoczyk, G. M. (2018). Slab2, a comprehensive subduction zone geometry model. *Science*, *362*(6410), 58–61. https://doi.org/10.1126/science.aat4723

He, B., Wei, X. Z., Wei, M., Shen, Y., Alvarez, M., & Schwartz, S. Y. (2023). A shallow slow slip event in 2018 in the Semidi segment of the Alaska subduction zone detected by machine learning. *Earth and Planetary Science Letters*, *612*. https://doi.org/10.1016/j.epsl.2023.118154

Herman, M. W., & Furlong, K. P. (2021). Triggering an unexpected earthquake in an uncoupled subduction zone. *Science Advances*, *7*(13), eabf7590. https://doi.org/10.1126/sciadv.abf7590

Hilde, T. W. C. (1983). Sediment subduction versus accretion around the pacific. *Tectonophysics*, *99*, 381–397. https://doi.org/10.1016/0040-1951(83)90114-2

Hirano, N. (2011). Petit-spot volcanism: A new type of volcanic zone discovered near a trench. *Geochemical Journal*, *45*, 157–167. https://doi.org/10.2343/geochemj.1.0111

Hirano, N., Takahashi, E., Yamamoto, J., Abe, W., Ingle, S. P., Kaneoka, I., Hirata, T., Kimura, J. I., Ishii, T., Ogawa, Y., Machida, S., & Suyehiro, K. (2006). Volcanism in response to plate flexure. *Science*, *313*, 1426–1428. https://doi.org/10.1126/science.1128235

Holt, A. F., Buffett, B. A., & Becker, T. W. (2015). Overriding plate thickness control on subducting plate curvature. *Geophysical Research Letters*, *42*(10), 3802–3810. https://doi.org/10.1002/2015GL063834

Hyndman, R. D., & Peacock, S. M. (2003). Serpentinization of the forearc mantle. *Earth and Planetary Science Letters*, *212*, 417–432. https://doi.org/10.1016/S0012-821X(03)00263-2

Ivandic, M., Grevemeyer, I., Berhorst, A., Flueh, E. R., & McIntosh, K. (2008). Impact of bending related faulting on the seismic properties of the incoming oceanic plate offshore of Nicaragua. *Journal of Geophysical Research*, *113*, B05410. https://doi.org/10.1029/2007JB005291

Iyer, K., Rüpke, L. H., Morgan, J. P., & Grevemeyer, I. (2012). Controls of faulting and reaction kinetics on serpentinization and double Benioff zones. *Geochemistry, Geophysics, Geosystems*, *13*(9), Q09010. https://doi.org/10.1029/2012GC004304

Jiang, Y., González, P. J., & Bürgmann, R. (2022). Subduction earthquakes controlled by incoming plate geometry: The 2020 M > 7.5 Shumagin, Alaska, earthquake doublet. *Earth and Planetary Science Letters*, *584*, 117447. https://doi.org/10.1016/j.epsl.2022.117447

Kita, S., Okada, T., Nakajima, J., Matsuzawa, T., & Hasegawa, A. (2006). Existence of a seismic belt in the upper plane of the double seismic zone extending in the along-arc direction at depths of 70-100 km beneath NE Japan. *Geophysical Research Letters*, *33*(24), L24310. https://doi.org/10.1029/2006GL028239

Kobayashi, K., Nakanishi, M., Tamaki, K., & Ogawa, Y. (1998). Outer slope faulting associated with the western Kuril and Japan trenches. *Geophysical Journal International*, *134*(2), 356–372. https://doi.org/10.1046/j.1365-246X.1998.00569.x

Kobayashi, K., Tamaki, K., Nakanishi, M., Korenaga, J., & Ogawa, Y. (1995). Rejuvenation of 130 m.y.-old Fabrics on the Outer Wall of the Western Kuril Trench. *Proceedings of the Japan Academy*, *71*(B), 5–9.

Korenaga, J. (2017). On the extent of mantle hydration caused by plate bending. *Earth and Planetary Science Letters*, *457*, 1–9. https://doi.org/10.1016/j.epsl.2016.10.011

Kuehn, H. (2019). *Along-trench segmentation and down-dip limit of the seismogenic zone at the eastern Alaska-Aleutian subduction zone* [PhD]. Dalhousie University, Halifax, Nova Scotia.

Lay, T., Ammon, C. J., Kanamori, H., Kim, M. J., & Xue, L. (2011). Outer trench-slope faulting and the 2011 Mw 9.0 off the Pacific coast of Tohoku Earthquake. *Earth, Planets and Space*, *63*(37), 713–718. https://doi.org/10.5047/eps.2011.05.006

Lay, T., Kanamori, H., Ammon, C. J., Hutko, A. R., Furlong, K., & Rivera, L. (2009). The 2006-2007 Kuril Islands great earthquake sequence. *Journal of Geophysical Research*, *114*, B11308. https://doi.org/10.1029/2008JB006280

Lefeldt, M., Ranero, C. R., & Grevemeyer, I. (2012). Seismic evidence of tectonic control on the depth of water influx into incoming oceanic plates at subduction trenches. *Geochemistry, Geophysics, Geosystems*, *13*(5), Q05013. https://doi.org/10.1029/2012GC004043

Li, J., Shillington, D. J., Bécel, A., Nedimović, M. R., Webb, S. C., Saffer, D. M., Keranen, K. M., & Kuehn, H. (2015). Downdip variations in seismic reflection character: Implications for fault structure and seismogenic behavior in the Alaska subduction zone. *Journal of Geophysical Research: Solid Earth*, *120*, 7883–7904. https://doi.org/10.1002/2015JB012338

Li, J., Shillington, D. J., Saffer, D. M., Bécel, A., Nedimović, M. R., Kuehn, H., Webb, S. C., Keranen, K. M., & Abers, G. A. (2018). Connections between subducted sediment, pore-fluid pressure, and earthquake behavior along the Alaska megathrust. *Geology*, *46*(4), 299–302. https://doi.org/10.1130/G39557.1

Li, S., & Freymueller, J. T. (2018). Spatial Variation of Slip Behavior Beneath the Alaska Peninsula Along Alaska-Aleutian Subduction Zone. *Geophysical Research Letters*, *45*, 3453–3460. https://doi.org/10.1002/2017GL076761

Liu, C., Lay, T., & Xiong, X. (2022). The 29 July 2021 M W 8.2 Chignik, Alaska Peninsula Earthquake Rupture Inferred From Seismic and Geodetic Observations: Re-Rupture of the Western 2/3 of the 1938 Rupture Zone. *Geophysical Research Letters*, *49*, e2021GL096004. https://doi.org/10.1029/2021gl096004

Lonsdale, P. (1988). Paleogene history of the Kula plate,: Offshore evidence and onshore implication. *Geological Society of America Bulletin*, *100*, 733–754. https://doi.org/10.1130/0016-7606(1988)100<0733:PHOTKP>2.3.CO;2

López, A. M., & Okal, E. A. (2006). A seismological reassessment of the source of the 1946 Aleutian "tsunami" earthquake. *Geophysical Journal International*, *165*(3), 835–849. https://doi.org/10.1111/j.1365-246X.2006.02899.x

Macdonald, K. C., Fox, P. J., Alexander, R. T., Pockalny, R., & Gente, P. (1996). Volcanic growth faults and the origin of Pacific abyssal hills. *Nature*, *380*, 125–129.

Masson, D. G. (1991). Fault patterns at outer trench walls. *Marine Geophysical Researches*, *13*, 209–225. https://doi.org/10.1007/BF00369150

Matulka, P., Wiens, D. A., Li, Z., Barcheck, G., Abers, G. A., & Ruppert, N. (2022). Along-strike Variation in Plate-bending Seismicity and Relationship to the Seismic Cycle in the Alaska Subduction Zone. *Seismological Research Letters*, *93*, 1299 (abstract).

Maus, S., Barckhausen, U., Berkenbosch, H., Bournas, N., Brozena, J., Childers, V., Dostaler, F., Fairhead, J. D., Finn, C., Von Frese, R. R. B., Gaina, C., Golynsky, S., Kucks, R., Lühr, H., Milligan, P., Mogren, S., Müller, R. D., Olesen, O., Pilkington, M., … Tontini, F. C. (2009). EMAG2: A 2-arc min resolution Earth Magnetic Anomaly Grid compiled from satellite, airborne, and marine magnetic measurements. *Geochemistry, Geophysics, Geosystems*, *10*, Q08005. https://doi.org/10.1029/2009GC002471

Miller, N. C., Lizarralde, D., Collins, J. A., Holbrook, W. S., & Van Avendonk, H. J. A. (2021). Limited Mantle Hydration by Bending Faults at the Middle America Trench. *Journal of Geophysical Research: Solid Earth*, *126*, e2020JB020982. https://doi.org/10.1029/2020JB020982

Mortera-Gutiérrez, C. A., Scholl, D. W., & Carlson, R. L. (2003). Fault trends on the seaward slope of the Aleutian Trench: Implications for a laterally changing stress field tied to a westward increase in oblique convergence. *Journal of Geophysical Research*, *108*(B10), 2477. https://doi.org/10.1029/2001JB001433

Naliboff, J. B., Billen, M. I., Gerya, T., & Saunders, J. (2013). Dynamics of outer-rise faulting in oceanic-continental subduction systems. *Geochemistry, Geophysics, Geosystems*, *14*(7), 2310–2327. https://doi.org/10.1002/ggge.20155

Nishikawa, T., & Ide, S. (2015). Background seismicity rate at subduction zones linked to slab-bending-related hydration. *Geophysical Research Letters*, *42*(17), 7081–7089. https://doi.org/10.1002/2015GL064578

Obana, K., Fujie, G., Takahashi, T., Yamamoto, Y., Tonegawa, T., Miura, S., & Kodaira, S. (2019). Seismic velocity structure and its implications for oceanic mantle hydration in the trench-outer rise of the Japan Trench. *Geophysical Journal International*, *217*(3), 1629–1642. https://doi.org/10.1093/gji/ggz099

Ogawa, Y., Kobayashi, K., Hotta, H., & Fujioka, K. (1997). Tension cracks on the oceanward slopes of the northern Japan and Mariana Trenches. *Marine Geology*, *141*, 111–123. https://doi.org/10.1016/S0025-3227(97)00059-5

Peacock, S. M. (2001). Are the lower planes of double seismic zones caused by serpentine dehydration in subducting oceanic mantle? *Geology*, *29*(4), 299–302. https://doi.org/10.1130/0091-7613(2001)029<0299:ATLPOD>2.0.CO;2

Pérez-Gussinyé, M., Lowry, A. R., Phipps Morgan, J., & Tassara, A. (2008). Effective elastic thickness variations along the andean margin and their relationship to subduction geometry. *Geochemistry, Geophysics, Geosystems*, *9*(2). https://doi.org/10.1029/2007GC001786

Petersen, S. E., Hoisch, T. D., & Porter, R. C. (2021). Assessing the Role of Water in Alaskan Flat-Slab Subduction. *Geochemistry, Geophysics, Geosystems*, *22*(5). https://doi.org/10.1029/2021GC009734

Polet, J., & Kanamori, H. (2000). Shallow subduction zone earthquakes and their tsunamigenic potential. *Geophysical Journal International*, *142*(3), 684–702. https://doi.org/10.1046/j.1365-246X.2000.00205.x

Protti, M., Güendel, F., & McNally, K. (1994). Correlation between the age of the subducting Cocos plate and the geometry of the Wadati-Benioff zone under Nicaragua and Costa Rica. *Physics of the Earth and Planetary Interiors*, *84*, 271–287. https://doi.org/10.1130/SPE295-p309

Ranero, C. R., Morgan, J. P., McIntosh, K., & Relchert, C. (2003). Bending-related faulting and mantle serpentinization at the Middle America trench. *Nature*, *425*, 367–373. https://doi.org/10.1038/nature01961

Ranero, C. R., Villaseñor, A., Morgan, J. P., & Weinrebe, W. (2005). Relationship between bend-faulting at trenches and intermediate-depth seismicity. *Geochemistry, Geophysics, Geosystems*, *6*(12), Q12002. https://doi.org/10.1029/2005GC000997

Ruff, L. J. (1989). Do Trench Sediments Affect Great Earthquake Occurrence in Subduction Zones? *Pageoph*, *129*, 263–282.

Ryan, W. B. F., Carbotte, S. M., Coplan, J. O., O'Hara, S., Melkonian, A., Arko, R., Weissel, R. A., Ferrini, V., Goodwillie, A., Nitsche, F., Bonczkowski, J., & Zemsky, R. (2009). Global multi-resolution topography synthesis. [Dataset]. *Geochemistry, Geophysics, Geosystems*, *10*(3). https://doi.org/10.1029/2008GC002332

Saffer, D. M., & Tobin, H. J. (2011). Hydrogeology and mechanics of subduction zone forearcs: Fluid flow and pore pressure. *Annual Review of Earth and Planetary Sciences*, *39*, 157–186. https://doi.org/10.1146/annurev-earth-040610-133408

Saffer, D. M., & Wallace, L. M. (2015). The frictional, hydrologic, metamorphic and thermal habitat of shallow slow earthquakes. *Nature Geoscience*, *8*(8), 594–600. https://doi.org/10.1038/ngeo2490

Scanlon, K. M., & Masson, D. G. (1992). Fe-Mn nodule field indicated by GLORIA, north of the Puerto Rico Trench. *Geo-Marine Letters*, *12*, 208–213. https://doi.org/10.1007/BF02091840

Sella, G. F., Dixon, T. H., & Mao, A. (2002). REVEL: A model for Recent plate velocities from space geodesy. *Journal of Geophysical Research: Solid Earth*, *107*(B4), ETG 11-1-ETG 11-30. https://doi.org/10.1029/2000jb000033

Sharples, W., Jadamec, M. A., Moresi, L. N., & Capitanio, F. A. (2014). Overriding plate controls on subduction evolution. *Journal of Geophysical Research: Solid Earth*, *119*(8), 6684–6704. https://doi.org/10.1002/2014JB011163

Shillington, D. J., Bécel, A., Nedimovic, M. R., Kuehn, H., Webb, S. C., Abers, G. A., Keranen, K. M., Li, J., Delescluse, M., & Mattei-Salicrup, G. A. (2015). Link between plate fabric, hydration and subduction zone seismicity in Alaska. *Nature Geoscience*, *8*, 961–964. https://doi.org/10.1038/ngeo2586

Smith, D. K., Schouten, H., Zhu, W. L., Montési, L. G. J., & Cann, J. R. (2011). Distributed deformation ahead of the Cocos-Nazca Rift at the Galapagos triple junction. *Geochemistry, Geophysics, Geosystems*, *12*(11), Q11003. https://doi.org/10.1029/2011GC003689

Stevenson, A. J., Scholl, D. W., & Vallier, T. L. (1983). Tectonic and geologic implications of the Zodiac fan, Aleutian Abyssal Plain, northeast Pacific. *Geological Society of America Bulletin*, *94*, 259–273. https://doi.org/10.1130/0016-7606(1983)94<259:TAGIOT>2.0.CO;2

Straume, E. O., Gaina, C., Medvedev, S., Hochmuth, K., Gohl, K., Whittaker, J. M., Abdul Fattah, R., Doornenbal, J. C., & Hopper, J. R. (2019). GlobSed: Updated Total

Sediment Thickness in the World’s Oceans. *Geochemistry, Geophysics, Geosystems*, *20*, 1756–1772. https://doi.org/10.1029/2018GC008115

Triezenberg, P. J., Hart, P. E., & Childs, J. R. (2016). [Dataset]. *National Archive of Marine Seismic Surveys (NAMSS): A USGS data website of marine seismic reflection data within the U.S. Exclusive Economic Zone (EEZ): U.S. Geologic Survey Data Release*.

Valentine, G. A., & Hirano, N. (2010). Mechanisms of low-flux intraplate volcanic fields - Basin and Range (North America) and northwest Pacific Ocean. *Geology*, *38*(1), 55–58. https://doi.org/10.1130/G30427.1

Van Avendonk, H. J. A., Holbrook, W. S., Lizarralde, D., & Denyer, P. (2011). Structure and serpentinization of the subducting Cocos plate offshore Nicaragua and Costa Rica. *Geochemistry, Geophysics, Geosystems*, *12*(6). https://doi.org/10.1029/2011GC003592

Van Keken, P. E., Hacker, B. R., Syracuse, E. M., & Abers, G. A. (2011). Subduction factory: 4. Depth-dependent flux of H2O from subducting slabs worldwide. *Journal of Geophysical Research: Solid Earth*, *116*, B01401. https://doi.org/10.1029/2010JB007922

von Huene, R., Miller, J. J., & Weinrebe, W. (2012). Subducting plate geology in three great earthquake ruptures of the western Alaska margin, Kodiak to Unimak. *Geosphere*, *8*(3), 628–644. https://doi.org/10.1130/GES00715.1

Wang, K., & Bilek, S. L. (2014). Invited review paper: Fault creep caused by subduction of rough seafloor relief. *Tectonophysics*, *610*, 1–24. https://doi.org/10.1016/j.tecto.2013.11.024

Wei, S. S., Ruprecht, P., Gable, S. L., Huggins, E. G., Ruppert, N., Gao, L., & Zhang, H. (2021). Along-strike variations in intermediate-depth seismicity and arc magmatism along the Alaska Peninsula. *Earth and Planetary Science Letters*, *563*, 116878. https://doi.org/10.1016/j.epsl.2021.116878

Worthington, L. L., Van Avendonk, H. J. A., Gulick, S. P. S., Christeson, G. L., & Pavlis, T. L. (2012). Crustal structure of the Yakutat terrane and the evolution of subduction and collision in southern Alaska. *Journal of Geophysical Research: Solid Earth*, *117*, B01102. https://doi.org/10.1029/2011JB008493

Xiao, Z., Freymueller, J. T., Grapenthin, R., Elliott, J. L., Drooff, C., & Fusso, L. (2021). The deep Shumagin gap filled: Kinematic rupture model and slip budget analysis of the 2020 Mw 7 . 8 Simeonof earthquake constrained by GNSS , global seismic waveforms , and floating InSAR. *Earth and Planetary Science Letters*, *576*, 117241. https://doi.org/10.1016/j.epsl.2021.117241

Yang, L., Wang, J., & Xu, C. (2023). Coseismic Coulomb stress changes induced by a 2020–2021 MW > 7.0 Alaska earthquake sequence in and around the Shumagin gap and its influence on the Alaska-Aleutian subduction interface. *Geodesy and Geodynamics*. https://doi.org/10.1016/j.geog.2023.04.007

Zhao, B., Bürgmann, R., Wang, D., Zhang, J., Yu, J., & Li, Q. (2022). Aseismic slip and recent ruptures of persistent asperities along the Alaska-Aleutian subduction zone. *Nature Communications*, *13*(3098). https://doi.org/10.1038/s41467-022-30883-7

Zhou, Y., Wang, W., He, J., Wang, X., Pan, Z., & Zhao, G. (2022). The 19 October 2020 Mw 7.6 Earthquake in Shumagin, Alaska: An Unusual Dextral Strike-Slip Event. *Pure and Applied Geophysics*, *179*, 3527–3542. https://doi.org/10.1007/s00024